Università degli Studi di Padova

Dipartimento dei Beni Culturali: Archeologia,
Storia dell'Arte, del Cinema e della Musica

Laurea Magistrale in SCIENZE ARCHEOLOGICHE

Curriculum in
APPLIED SCIENCES TO CULTURAL HERITAGE MATERIALS AND SITES

"Mineralisation of ancient textiles: An archaeometric analysis of Etruscan textile fragments from the tombs of Perugia"

Supervisor:

Prof. Margarita Gleba

Co-supervisors:

Prof. Alfonso Zoleo

Prof. Gilberto Artioli

Master Candidate

Nina Janske Schuurman

2050902

ACADEMIC YEAR 2022/2023

This page is intentionally left blank

Table of Contents

Acknowledgements

First and foremost, I would like to express my deepest gratitude to prof. Margarita Gleba, without whom this thesis would not have seen the light of day. Not only did she provide the samples this thesis is centered around, she also generously shared her knowledge and expertise with me. I could not have undertaken this journey without her invaluable feedback and guidance.

I am also extremely grateful for the support from prof. Alfonso Zoleo, who graciously helped me with the Raman and FTIR-ATR analyses and interpretation. In the same vein, I would like to express my sincere gratitude to prof. Gilberto Artioli, who greatly assisted me with the XRD portion of this thesis. Without the support of both of these professors I would most definitely have been lost in the chemical analyses of the samples.

Special thanks should also go to Dr. Gregorio Dal Sasso for providing me access to the CLSM, and for always opening the doors to the labs for me without complaint.

Last but not least, I would like to acknowledge the love and support from my family and friends, in particular from my fellow master students and treasured friends Ciara McCarthy, Kiana Sokolic and Paula Stipanovic. I feel incredibly lucky that we ran into each other at UniPD, without them my time in Italy would not have the same!

Abstract

Ancient textiles do not appear often in the archaeological record, and when they do, they might have undergone chemical alteration, allowing them to survive through time. This process of mineralisation, where the organic fibres have been replaced, fully or partially, by inorganic compounds, has been known to occur when the textile has been in contact with a metal. However, another, more rare type of mineralisation occurs in calcium-rich environments. The textile samples from the late Etruscan (2nd-1st century BCE) cemeteries of Strozzacapponi and Ponticello near Perugia, Italy, discussed in this thesis present such a case. This thesis aims to uncover the mineralisation process these textile fragments have undergone, using various archaeometric techniques: Confocal laser scanning microscopy, portable and benchtop micro-Raman, Fourier-transform infrared spectroscopy and X-ray diffraction.

The analyses show that the main mineral components of the textile samples examined mostly consist of calcium carbonate (calcite) or gypsum. So far, no absolute cause could be determined. However, the use of travertine (a carbonate rock) as material for the cinerary urns might have had a significant influence on the mineralisation process, as well as the microclimate present within subterranean tombs. Furthermore, a recent hypothesis that the Etruscans could have added slaked lime to the contents of the urns is explored.

Sommario in Italiano

I tessuti antichi non compaiono spesso nel registro archeologico e, quando lo fanno, alcuni potrebbero aver subito alterazioni chimiche che permettono loro di sopravvivere nel tempo. Questo processo di mineralizzazione, in cui le fibre organiche sono state sostituite, completamente o parzialmente, da composti inorganici, è noto per verificarsi quando il tessuto è stato a contatto con un metallo. Tuttavia, un altro tipo di mineralizzazione più raro si verifica in ambienti ricchi di calcio. I campioni di tessuto provenienti dalle tombe tardo-etrusche (II-I secolo a.C.) dei cimiteri di Strozzacapponi e Ponticello vicino a Perugia, Italia, discussi in questa tesi, presentano un caso del genere. Esistono due ipotesi principali sulla causa della mineralizzazione. Una punta principalmente a cause di degradazione naturale in combinazione con l'abbondanza di minerali ricchi di calcio, l'altra suggerisce l'aggiunta di calce spenta come parte della tradizione funeraria del popolo. Nel tentativo di scoprire il processo di mineralizzazione a cui sono stati sottoposti questi frammenti, i minerali sono stati analizzati utilizzando varie tecniche archeometriche, come la microscopia a scansione laser confocale, la spettroscopia Raman portatile e microscopica, la spettroscopia infrarossa a trasformata di Fourier e infine la diffrazione dei raggi X. Oltre all'identificazione dei componenti minerali, questa tesi serve anche come esplorazione dell'applicazione di tali tecniche su campioni complessi come questi.

Materiali

I dieci campioni mineralizzati provengono da tre tombe: Tomba dei Satna (Ponticello, 7 campioni), Tomba 27 (Strozzacapponi, 1 campione) e Tomba 29 (Strozzacapponi, 2 campioni). Queste tombe sono tutte del tipo ipogeo a camera, tipiche del tarda età ellenistica risalente al II-I secolo a.C. e contengono urne cinerarie prodotte in travertino, un tipo di roccia carbonatica. Tutti tranne uno dei dieci campioni sono stati trovati all'interno di queste urne, solo il campione S03-40 (Tomba 29) è stato trovato sopra una delle urne. Questi campioni sono stati originariamente raccolti in associazione con il progetto Marie Curie FIBRE (Fibre in Italy Before Roman Empire), che si è svolto dal 2009 al 2011, da Margarita Gleba. Durante questa ricerca precedente, in cui è stata identificata la tecnologia tessile di questi frammenti mineralizzati, è stata rilevata la presenza di calcite e gesso utilizzando SEM-EDS.

Metodi

Tutte le immagini CLSM dei tessuti mineralizzati sono state registrate in modalità di riflessione utilizzando un Olympus LEXT OLS4100 situato presso il Dipartimento di Scienze della Terra dell'Università di Padova. Questo CLSM era dotato di cinque obiettivi (2,5x, 5x, 10x, 20x e 50x) e un laser a 405 nm. L'elaborazione e la compilazione delle immagini sono state effettuate utilizzando il pacchetto software Olympus LEXT OLS4100 versione 3.1.15. Per ottenere una buona panoramica delle superfici dei campioni, è stata utilizzata l'applicazione di stitching del software per combinare più immagini singole in una sola. Sono stati utilizzati due diversi setup Raman: uno spettrometro Raman portatile BWTEK inc. con un laser a 785 nm (rosso), accoppiato a un microscopio Optika Microscopes Italy, e uno spettrometro micro-Raman inVia Renishaw da banco, dotato di un laser a 514 nm (verde), accoppiato a un microscopio Leica Dm-LM. Entrambi questi setup Raman erano situati presso il Dipartimento di Scienze Chimiche dell'Università di Padova. L'analisi FTIR-ATR dei campioni è stata effettuata utilizzando uno spettrometro FTIR Bruker Optics mod. Alpa T dotato di un modulo Broker Optics platinum ATR QuickSnap™ e una piastra ATR in diamante, situato presso il Centro di Analisi e Servizi Per la Certificazione (CEASC) a Padova. Tutti gli spettri sono stati acquisiti con 32 scansioni, corretti ATR. L'analisi XRD sui campioni selezionati di tessuti mineralizzati è stata effettuata utilizzando un diffrattometro PANanlytical X'Pert PRO con geometria di Bragg Brentano in modalità di focalizzazione in trasmissione attraverso uno specchio dedicato, radiazione Cu K-alpha, rivelatore PIXcel e un supporto per campioni a rotazione riflessione-trasmissione, situato presso il Dipartimento di Scienze della Terra dell'Università di Padova.

Risultati

Durante l'analisi CLSM, i campioni sono stati raggruppati in 4 gruppi in base alle loro caratteristiche visive e efficacemente in 2 gruppi in base a quanto bene è stata preservata la struttura originale del tessuto. È diventato rapidamente chiaro che nessuna delle fibre organiche originali era ancora presente sulla superficie per nessuno dei campioni.

La spettroscopia Raman, sia portatile che da banco, ha riscontrato problemi dovuti alla fluorescenza. Durante il Raman portatile, è stata rilevata la presenza di gesso per tre campioni (P03-29, P07-33 e S01-45) e di calcite per uno (S06-38), per gli altri non è stato possibile ottenere uno spettro utilizzabile. La spettroscopia Raman da banco ha confermato questi risultati per i campioni P03-29, P07-33 e S01-45, anche se P07-33 potrebbe mostrare anche un po' di calcite e S06-38 non ha prodotto alcun risultato

utilizzabile. Inoltre, è stato rilevato anche il gesso per il campione P01-23. Fino ad ora tutti gli spettri Raman leggibili sono stati ottenuti da aree bianche, solo per il campione S03-40 è stato possibile ottenere uno spettro da un'area nera: questo ha prodotto uno spettro per il nero di carbonio.

I risultati FTIR-ATR sono in gran parte concordi con i risultati Raman per quanto riguarda il contenuto minerale, ad eccezione di P01-23, che durante il FTIR-ATR è risultato essere calcite. È diventato abbastanza evidente che ci sono due gruppi principali tra i campioni; uno che contiene principalmente gesso e uno che contiene principalmente calcite. C'è anche un valore anomalo con il campione P08-34, che sembra contenere principalmente aluminosilicati. Inoltre, FTIR-ATR ha rilevato residui organici per i campioni P05-31 e P08-34 e residui di cellulosa per i campioni P01-23, P02-27 e S03-40.

I risultati XRD sui campioni selezionati concordano con i risultati FTIR-ATR per quanto riguarda il contenuto minerale principale dei campioni. La metà dei campioni conteneva frazioni variabili di quarzo (P01-23, P07-33 e S03-40), con i campioni P01-23 e S03-40 che contenevano anche altre impurità non identificabili. Inoltre, il campione S06-38 contiene due diverse forme di calcite: calcite di magnesio e calcite. Poiché non tutti i risultati FTIR-ATR erano completi al momento della selezione per XRD, il campione P08-34 non è stato selezionato, anche se in retrospettiva sarebbe stato un buon candidato per l'analisi XRD.

Discussione

È chiaro, ad eccezione di un caso, che ci sono due gruppi principali da identificare tra questi campioni. Un gruppo contenente principalmente gesso (P03-29, P05-31, P07-33, P09-36 e S01-45) e un gruppo contenente principalmente (una forma di) calcite (P01-23, P02-27, S03-40 e S06-38). La causa di questa differenza non è stata identificata. Questi due gruppi non sembrano corrispondere alla tecnologia tessile dei frammenti identificati negli studi precedenti, né sono necessariamente specifici delle tombe poiché campioni provenienti dalla Tomba dei Satna sono presenti in entrambi i gruppi.

Le due ipotesi principali su ciò che ha causato la mineralizzazione non hanno potuto essere provate o confutate. L'alterazione fisico-chimica potrebbe essere avvenuta nei microclimi specifici delle tombe, causando l'efflorescenza. Inoltre, studi sulla colonizzazione microbica di tombe simili indicano la presenza di batteri che possono causare croste di calcite. Tuttavia, non si sa se tali processi di degradazione abbiano avuto luogo nelle tombe da cui sono stati recuperati questi campioni.

L'aggiunta di calce spenta comporterebbe una forte carbonatazione, nonché la degradazione della cellulosa con la formazione di residui di cellulosa come quelli rilevati

con FTIR-ATR. Tuttavia, a causa della natura di FTIR-ATR, non è possibile sapere se questi residui di cellulosa siano resti della fibra originale o siano residui sulla superficie (contaminazione). Altri casi in cui i tessuti si sono mineralizzati in gesso e/o calcite provengono da contesti funerari dell'Età del Bronzo della Siria (Qatna) e del Libano (Sidone): potrebbe essere più probabile che l'ambiente delle tombe di questi reperti sia un fattore importante nel processo, piuttosto che condividano tutti una pratica di sepoltura simile. Entrambe le ipotesi spiegano principalmente la presenza di calcite, anche se la maggior parte dei campioni conteneva gesso.

Conclusioni

Le analisi svolte hanno dimostrato che questo tipo di mineralizzazione coinvolge principalmente gesso e calcite, anche se in un caso il minerale più prominente sembrava essere un aluminosilicato. La causa esatta di questo risultato rimane ancora poco chiara, poiché nessuna delle ipotesi discusse è stata (in)validata. È necessaria ulteriore ricerca riguardo ai fattori ambientali presenti intorno ai tessuti mineralizzati, nonché ulteriori prove chimiche e archeologiche sull'uso della calce spenta.

CHAPTER 1:

Introduction

Textiles do not often appear within the archaeological record, even though they have been part of human history for quite some time. The earliest evidence of a twined textile appears in the Czech Republic, from the site Pavlov I, where impressions of textiles on clay can be dated to circa 26.000 years ago (Adovasio J. M., Soffer O., & Klíma B. 1996). Textiles, aside from being used for clothing, have played multiple roles within society – think of fishnets, sails, and shelters – and are important in our understanding of past societies and its peoples. Unfortunately, due to the organic nature of the fibres used for textile production, textiles, more often than not, deteriorate rapidly once left to their own devices (Jakes K.A. & Sibley L.R. 1984).

There are some environments in which textiles are able withstand the test of time, such as very dry desert environments, especially in combination with salt: Think of textiles from the tomb of Tutankhamun (Hoskins N.A. 2011), Roman Egyptian sites such as Mons Claudianus (Bender Jørgensen L. 2004) and later Coptic materials that have all survived in Egypt due to its dry climate (Han J.I. 2011). This phenomenon is not unique to the Egyptian desert of course, as textiles have also been recovered from the tower tombs of Roman-era Palmyra in Syria (Schmidt-Colinet A. 1995), as well as textiles still being present wrapped around the pre-Columbian mummies of the Atacama Desert (Conklin W.J. & Conklin B.M. 2007) and on the mummified bodies found buried in the Tarim Basin (Gleba M. & Mannering U. 2012; Zhang X., Good I., Laursen R. 2008).

Desiccation is not the only way in which textiles can be well preserved, the complete opposite environment of waterlogging can prevent oxidation of the fibres from taking place (Good I. 2001). A great example of this type of preservation are textiles from various Bronze Age burial mounds in Denmark, which were waterlogged at the core (Frei K. M., Mannering U., Berghe I. V. & Kristiansen K. 2017; Mannering U., Possnert G., Heinemeier J. & Gleba M. 2010). Additionally, the acidic nature of the raised-bog environment on the Jutland peninsula adds to the capability of the preservation of proteinaceous materials, such as wool (Frei K. M., Mannering U., Berghe I. V. & Kristiansen K. 2017; Mannering U., Possnert G., Heinemeier J. & Gleba M. 2010; Good I. 2001). Cellulosic materials such as linen on the other hand abide better by an alkaline environment (Good I. 2001).

Waterlogging can also be beneficial in combination with permafrost (GOOD I. 2001; KING M.E. 1978). Various textile materials have survived within Iron Age burial mounds high up in the Altai mountains. Ironically, these textiles have been preserved so well due to the intervention of ancient grave robbers, who, in their search for riches damaged the wooden burial chambers causing water to seep in and freeze (RUBINSON K.S. 1990).

Such extreme conditions prevent the organic fibre from being broken down, mainly because they prevent oxidizing (waterlogging, permafrost) or hydrolysis (desiccation) reactions from taking place. There are however other ways that ancient textiles can be preserved, albeit in an altered state, caused by chemical degradation (GOOD I. 2001). This process replaces the original organic material of the textile fibres in question with inorganic compounds, but the general shape of the textile may remain in varying degrees (JAKES K.A. & SIBLEY L.R. 1984; GOOD I. 2001). In cases where conditions are optimal, it may even be possible to obtain information on the spin direction or even the type of fibres themselves (GOOD I. 2001). This chemical replacement process, also known as mineralisation, produces a type of textile find that are commonly referred to as pseudomorphs ("false forms") (JAKES K.A. & SIBLEY L.R. 1984; CHEN H. L., JAKES K. A. & FOREMAN D. W. 1998; GOOD I. 2001). Textile pseudomorphs are generally formed when the textile has been in contact with a metal, such as iron, copper, bronze, or silver (KING M.E. 1978), in combination with a damp environment (CHEN H. L., JAKES K. A. & FOREMAN D. W. 1998; CYBULSKA M. & MAIK J. 2007). Moisture will cause corrosion of the metal objects, which can either start to form on the surface of the fibre, resulting in a hollow pseudomorph, a negative cast, when the organic material disintegrates over time (CYBULSKA M. & MAIK J. 2007). Another possible contribution of metal corrosion to the textile preservation is caused by the release of metal ions into the soil during this process (CHEN H. L., JAKES K. A. & FOREMAN D. W. 1998). These metal ions, if abundant enough, become toxic to many micro-organisms, inhibiting the microbiological degradation of the organic materials (CHEN H. L., JAKES K. A. & FOREMAN D. W. 1998). Such toxic metals include copper, nickel, mercury, and lead. These can be naturally present in the soil, albeit in very small quantities; it is rather buried metal objects that increase their concentration within the soil, hindering the microbial degradation processes (CHEN H. L., JAKES K. A. & FOREMAN D. W. 1998). These metal ions do not only impede the microbial degradation process, but they can also fill in or impregnate the textile fibre, which in combination with the fibre's natural degradation can eventually (partially) replace the original organic compounds of the textile fibres, creating textile pseudomorphs, or positive casts (CHEN H. L., JAKES K. A. & FOREMAN D. W. 1998). Though many define pseudomorphs as being

completely replaced by inorganic compounds, it is actually not uncommon for some traces of organic material to be left within the matrix (GOOD I. 2001). It is also important to note that *generally* textile pseudomorphs form in contact with metal objects, but this phenomenon can also occur on ceramics or stone, though it is considerably more rare and its chemical mechanism is different (GOOD I. 2001; CYBULSKA M. & MAIK J. 2007). For instance, when calcium is present in the environment surrounding the textile remains, mineralisation seems to occur in the form of a calcium carbonate or gypsum cast (GLEBA M. & MANNERING U. 2012). Textiles mineralised in such a way provide an environment in which dyes can survive, unlike textile that underwent metal mineralisation (GLEBA M. & MANNERING U. 2012). Examples of this type of mineralisation can be found in Bronze Age burials in Qatna (Syria) and Sidon (Lebanon), on which dye analysis was still possible (GLEBA M. & GRIFFITHS D. 2011; JAMES, M. A., REIFARTH N., MUKHERJEE A. J., CRUMP M. P., GATES P. J., SANDOR P., ROBERTSON F., PFÄLZNER P. & EVERSHED R. P. 2009). The textile samples that are discussed and analysed in this thesis have seemingly mineralised in this unusual way as well.

Ten mineralised textile samples have been collected from two late Etruscan necropoleis, Ponticello and Strozzacapponi, in Perugia, Italy. This was done as part of the Marie Curie project FIBRE (Fibre in Italy Before Roman Empire), conducted in 2009-2011 by prof. Margarita Gleba. This project's main aim was to map ancient Italy's textile fibre development and to place these findings into a broader archaeological context. Additionally, a chemical dye analysis of the samples from the Strozzacapponi necropolis was performed during the DressID (*Clothing and Identities – New Perspectives on Textiles in the Roman Empire*) project running from 2007-2012, using high-performance liquid chromatography with diode-array detection (HPLC-DAD). Additionally, using SEM-EDS the mineral composition was investigated. Additionally, using SEM-EDS the mineral composition was investigated.

This collection of textile samples, with the exception of one, originates from funerary urns that can be dated to the 2nd-1st century BCE. The cremated remains within these urns seemed to have been wrapped or placed on top of folded textiles, likely as part of the local funerary practises, though due to the highly advanced state of mineralisation it is unclear if these textiles were shrouds, garments, or other types of textiles (GLEBA M. & VANDEN BERGHE I. 2014). The finds and their state of preservation raise a series of questions: Is this mineralisation process caused by the environment these textile fragments were found in? Or are there other factors at play that could have led to this end result?

Initially, the use of travertine, a carbonate rock, as material for the cinerary urns seemed to be the main suspect for the calcification (GLEBA M., VANDEN BERGHE I. & CENCIAIOLI L. 2017). However, initial publications discussing the textile pseudomorphs from Strozzacapponi report that textiles have been mineralised into calcite *or* gypsum, or in some cases possibly a combination of both (GLEBA M. & VANDEN BERGHE I. 2014). If the travertine is the main cause of mineralisation, how could this process result in the occurrence of gypsum? And what if it is not strictly the environment of these textiles that causes this mineralisation, but instead it is influenced by human action?

At the International Workshop Archaeology and Archaeometry of Ancient Textiles: analytical methods, conservation, and dissemination in textile research, held at the Department of Scienze dell'Antichità, Sapienza University of Rome, 9th-10th June 2022, Nicole Reifarth suggested that mineralisation in the presence of calcium may be due to people intentionally adding slaked lime (calcium hydroxide) to the burials as part of funerary rituals (Pers. Comm. Margarita Gleba). This might explain the reoccurring presence of calcium carbonate (calcite) in multiple instances, however, there might be some trouble in regard to this hypothesis when gypsum is present as well. Furthermore, is it possible to detect a difference between mineralisation caused by the intentional addition of slaked lime and mineralisation due to natural causes? Additionally, many other factors might have influenced the process of mineralisation, for instance the original fibre of the textile, or perhaps the dyes and mordants used to colour them.

In order to shed more light on the mineralisation process that has occurred on these textile samples from Perugia, multiple archaeometric analytical techniques were applied toward identifying the mineral phases present on the samples, as well as the degree of preservation of the organic material in an attempt to identify the original fibre. These techniques include various types of Raman spectroscopy as well as Fourier transform infrared spectroscopy (FTIR), which are used to uncover the chemical compositions of the samples in order to determine which minerals are present. These techniques are also capable, in varying degrees of accuracy, to detect organic functional groups, making it possible to determine if the textile fibre is plant or animal based. Lastly, in order to obtain crystallographic information on the mineral phases the samples were subjected to X-ray diffraction. Combining these data will give us some insight into the processes at hand.

CHAPTER 2:

Archaeological context

Archaeology never exists in a vacuum. This, of course, also applies to these mineralised textile fragments, which were once part of people's cultural traditions. This chapter will therefore provide a short overview of Etruscan civilization as well as their funerary practices, as these fragments were retrieved from a funerary context. Lastly, the city of Perugia will be discussed along with the specific contexts of the samples, in order to help us understand the environment in which these textiles were preserved in a mineralised state.

2.1 Ancient Etruria

Etruscan civilization managed to occupy quite a sizable portion of ancient Mediterranean history, spanning about 9 centuries in total (HAYNES S. 2000). Its origin is associated with the Iron Age Villanovan culture, which is regarded as an early period of Etruscan culture that flourished from the 10th until the 8th century BCE (HAYNES S. 2000). However, one must not forget that a considerable number of other ethnic, cultural, geographic, political, and linguistic factors contributed to the formation of their culture as well (HAYNES S. 2000). The Etruscan culture is mainly focussed in an area nestled between the Tyrrhenian Sea to the west, and the Arno and Tiber Rivers to the north and south respectively (HAYNES S. 2000; WIMAN I.M.B. 2014). Along the coasts of this area the landscape consists of plains but move more inland and it changes to a rough landscape of hills, running both east–west and north–south (SMITH C. 2014). This rugged landscape has been formed by water, limestone, and ancient volcanic activity, and knows agriculturally fertile parts, as well as parts rich in mineral resources such as silver, copper, and lead among others (SMITH C. 2014). In the course of time, the Etruscans spread out to the northeast, to the Po valley, where the trade cities of Spina and Adria were founded on the Adriatic coast during the 6th century BCE (WIMAN I.M.B. 2014). The Etruscan sphere of influence at some points included large parts of Latium, which during the 6th century BCE also included a young Rome (WIMAN I.M.B. 2014). It is important to note however, that the area occupied by the Etruscans is not one cohesive unit, but rather a collection of independent Etruscan cities with slight but notable differences in art and customs between them (BANTI L. 1973;

HAYNES S. 2000). These cities formed a loose network of settlements controlling their surrounding territories in the countryside (HAYNES S. 2000; SMITH C. 2014). According to Livy, Etruscan cities and their leaders held annual assemblies at the sanctuary of Fanum Voltumnae for religious celebrations and games, much like the Greeks did in Olympia (HAYNES S. 2000).

Etruscan cities are often located on either volcanic tufa plateaus – as is usually the case for the cities of southern Etruria and Lazio (such as Veii, Tarquinia, Vulci and Orvieto) – or, as seen in the central and northern regions, they are commonly located on top of hills near the sea or waterways (such as Populonia, Vetulonia, Pisa, Volterra, Chiusi, Cortona and Arezzo) (HAYNES S. 2000). Though this is not a set rule that every Etruscan city follows of course, as is the case with the city of Perugia, a city that will be more thoroughly discussed later in this chapter.

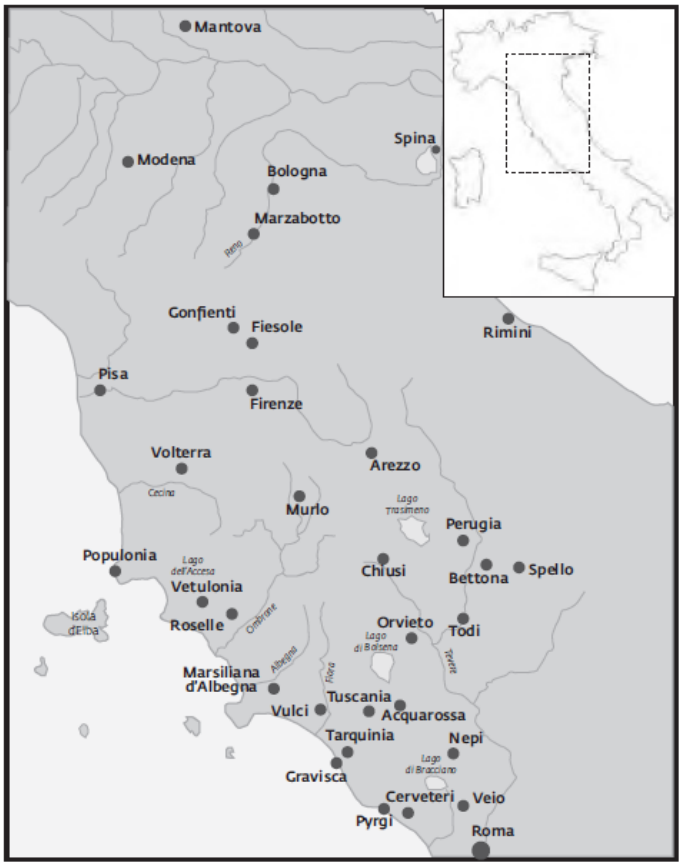

Figure 1: Map featuring major Etruscan cities (from: BARTOLONI G. 2012, page 17).

As Etruscan civilization covered such a long period of time, many different cultural developments and periods can be observed throughout its existence (HAYNES S. 2000). After the initial Villanovan period during the Early Iron Age, the Etruscans came into contact with Phoenicians and the Greeks, who settled on the Italian peninsula during the

8th century BCE (SMITH C. 2014). With them came new developments and concepts in art, architecture, religious expression, and a new alphabet, which the Etruscans readily adopted (SMITH C. 2014). This period is dubbed the Orientalizing period, as the push for all these innovations are believed to have been brought over by peoples coming from the east (SMITH C. 2014). The urbanization of Etruscan settlements and the imported luxury items that accompanied the richly decorated tombs are clear indications of a booming period of intricate trade networks and connections (HAYNES S. 2000). This richness in art and trade continued into the Archaic period where urbanization and the fruitful trade connections gave rise to social changes, allowing merchants, manufacturers, and craftsmen to accumulate amounts of wealth comparable to that of the ruling class (HAYNES S. 2000). However, the rise of conflict during this period and the centuries that follow, both originating within Etruria as well as from outside forces, started to slow down innovation and decreased the area under Etruscan rule (SMITH C. 2014). Especially cities in the southern regions of Etruria were affected by the subsequent loss of trade routes and unrest in Lazio and Campania, causing economic decline (HAYNES S. 2000). Though the mineral-rich northern coastal cities suffered naval attacks by Syracusans, who managed to greatly expand their power in the region during the 5th century BCE, they managed to continue to flourish (HAYNES S. 2000). From the 4th century BCE onward, pressure from the Romans started to pick up, starting with the inland cities (HAYNES S. 2000; SMITH C. 2014). Interestingly, the coastal cities of Ceveteri and Tarquinia experienced a resurgence in creativity and wealth during this time (HAYNES S. 2000). As with many cultural groups occupying the Italian Peninsula – and ultimately the greater Mediterranean sphere – it got slowly but steadily incorporated into the Roman Republic from the fourth to the first century BCE (HAYNES S. 2000). Eventually, with the rise of the Roman Empire under emperor Augustus came the definitive end of their distinct culture (BARTOLONI G. 2012).

PERIODS WITHIN ETRUSCAN CIVILIZATION	
Villanovan period/ Early iron age	900 - 720 BCE
Orientalizing period	720 - 580 BCE
Archaic period	580 - 480 BCE
Classical period	480 - 320 BCE
Hellenistic period	320 - 27 BCE

Table 1: Chronological overview of the main periods recognized within Etruscan civilization (after: BARTOLONI G. 2012, pages 8-16)

2.2 Etruscan necropoleis and funerary practises

When discussing the Etruscans and their civilization, most of what we know we have learned from their tombs and grave goods (HAYNES S. 2000; STEINGRÄBER S. 2016). Since most of the important Etruscan cities are still inhabited to this day it makes excavating them difficult, as modern buildings and infrastructure cover the ancient layers (HAYNES S. 2000). Etruscan necropoleis on the other hand were customarily located outside of the cities, making them still accessible to this day, and on top of that, Etruscan tombs are generally constructed out of lasting materials and enjoy a more massive architecture compared to other buildings (STEINGRÄBER S. 2016).

Since Etruscan civilization stretched for nearly a millennium and was organized as independent cities, there is no standard funerary practise that is applicable to all time periods and settlements. There are, however, some broad trends that can be identified. Starting with the Villanovan period where the overarching funerary rite resembled that of the Urnfield Culture of Central Europe, with cremation burials consisting of biconical ceramic urns or urns with helmet shaped lids, though the most iconic early iron age urn type are the house or hut urns, who appear mainly in southern Etruria and Latium (HAYNES S. 2000; LEIGHTON R. 2005). As the name suggests, these urns resemble the homes of the living and seem to have been reserved for individuals of higher status (HAYNES S. 2000; LEIGHTON R. 2005). The tombs in question were fairly simple: They consisted of a stone covered, deep, cylindrical pit carved into the rock or earth inside of which the urns were placed (HAYNES S. 2000). During this period, grave goods were relatively few in number and quite modest, as the status of the individual more likely expressed by the quality of the goods instead of the quantity (HAYNES S. 2000). Typically, members of the same familial group appear clustered together, a trend that can still be observed in the 7th century BCE in the form of large chamber tombs in which multiple generations of a family are laid to rest (HAYNES S. 2000; STEINGRÄBER S. 2020).

The development of such chamber tombs came with the practise of inhumation, a practise of which the slow rise can be seen as early as the late 9th century BCE in Populonia (HAYNES S. 2000). These very early chamber tombs have a ceiling constructed out of limestone slabs, forming a false vault, as well as a short, stone-lined corridor (*dromos*) as a means of access to the chamber (HAYNES S. 2000). In other Etruscan cities chamber tombs were carved out from the rock if the geology allowed for it (STEINGRÄBER S. 2020).

By the time the Orientalizing period rolled around the practice of inhumation became more widespread, especially among the elites, though the cremation tradition remains present – in varying degrees – alongside inhumation (HAYNES S. 2000). Inhumation entailed the placement of the deceased on a stone bed or in a stone or wooden sarcophagus, and around this time the burial was accompanied by a whole array of rich burial goods (STEINGRÄBER S. 2016).

Many different types of tombs and construction methods started to develop, partially determined by geological and geographical parameters, and partially by local tradition (STEINGRÄBER S. 2020). Among the most common tomb types are the early well/ pit tombs (for cremation burials) & fossa tombs, loculus tombs, niche tombs, chamber tombs, cassone tombs (mainly in Vulci), house tombs, and stone cist tombs, among many more – all with their own regional variations (IZZET V. 2007; STEINGRÄBER S. 2016; STEINGRÄBER S. 2020). The house tomb in an interesting type, as it seems to preserve the house iconography of the house urns of earlier periods, with its painted or stuccoed architectural elements within the tomb, mirroring houses of the living (HAYNES S. 2000; LEIGHTON R. 2005; STEINGRÄBER S. 2020).

There are in general two main ways Etruscan tombs are constructed: They are built using stone slabs from either tufa, limestone, or sandstone (most common in northern regions), or they are carved directly into the local rock (most common in the south) (HAYNES S. 2000; STEINGRÄBER S. 2020). Furthermore, where the first chamber tombs were covered by a low mound, the later ones were covered by enormous cylindrical tumuli, which could reach up to 12 -15 meters in height and 30 - 40 meters in diameter (HAYNES S. 2000).

With the eventual rise of the "middle classes" during 6th century BCE, smaller, simpler, and more unified tombs within various Etruscan necropoleis started to appear (HAYNES S. 2000; IZZET V. 2007). A good example for this phenomenon is the sober and rectangular or cubic tombs that can be found in necropoleis of Cerverteri, Veii and Marzabotto, which are all organized within regular orthogonal street plans, contrasting with the haphazard placement of the large aristocratic tumili in the period prior (HAYNES S. 2000; IZZET V. 2007; STEINGRÄBER S. 2020). However, as is often the case with Etruscan customs, this trend does not appear everywhere. On the contrary, the iconic painted chamber tombs slowly started to appear in Tarquinia (although still on a small scale) around the same time (HAYNES S. 2000).

As discussed before, the rise of conflict during the latter half of the Archaic period and into the Classical period caused economic decline for the majority of Etruscan cities (HAYNES S. 2000). This is reflected in the diminished amount of foreign goods within the grave good

assemblages, as well as the poorer quality of the local ware and decorations of the tombs (HAYNES S. 2000).

The production of high-quality funerary goods picks up again during the fourth century BCE, when skillfully carved high-relief sarcophagi appear in the Ponte Rotto necropolis of Vulci, as well as in Tarquinia (HAYNES S. 2000). From the second half of the fourth century onwards large aristocratic chamber tombs in these cities are decorated with high quality wall-paintings, along with the occasional painted sarcophagus, suggesting an economic, as well as political revival despite the rise of Rome (HAYNES S. 2000; STEINGRÄBER S. 2020). However, the gradual replacement of cremation with inhuman did not occur in all regions occupied by the Etruscans (STODDART S. 2016a). Communities in the northeast of Etruria kept the cremation tradition from the early Iron Age to well into the Roman period (STODDART S. 2016a). Perugia, and especially Chiusi, were centres where cremation was the primary practise throughout the centuries as well (STODDART S. 2016a). Ash urns from Chiusi, made from alabaster, travertine, or clay, were often painted in vivid colours, and seem to have been mass produced from the second half of the second century onwards with the use of moulds (HAYNES S. 2000). These moulded urns seem to have been in use by people of the middle classes, and occasionally feature the deceased on top of the lid in either a resting or banqueting position, as is often seen with the high-relief aristocratic sarcophagi that appear in other Etruscan cities, such as Tarquinia (HAYNES S. 2000).

In short, a lot of variation in funerary practices and architecture occur within the Etruscan territory, especially from the Villanovan period onwards. Important overarching distinctions that could be made are that in the southern regions, where the landscape commonly features (volcanic) rock outcrops, the tombs are commonly carved into the local stone, while in the northern regions, where the terrain is less rough, they are build using stone slabs of various types of rock (STEINGRÄBER S. 2016). Additionally, the gradual transition from cremation to inhumation did not occur in the same rate everywhere, or hardly at all in the case of northeastern Etruria (STODDART S. 2016a)

2.3 Perugia

Perugia is located on a hill along the western side of the Tiberino basin in the region of Umbria, marking the eastern limits of ancient Etruria (BIZZARRI R., MELELLI L. & CENCETTI C. 2018; HAYNES S. 2000). The city is surrounded by fairly rough terrain, with tall

limestone mountains peeking through the surrounding sandstone & marl hills to the north, while it overlooks the Tiber Valley to the south (STODDART S. 2016b). Eventually Perugia grew out to be one of the twelve confederate cities of the Etruscan league, largely due to its strategic location between main routes connecting various neighbouring cities, even though Perugia's urban centre seems to have developed significantly later than most of the other large Etruscan cities (BIZZARRI R., MELELLI L. & CENCETTI C. 2018; NEIL S. 2016).

Although much of the ancient city is located below the modern one, some archaeological evidence has been found for Villanovan habitation in the area, as well as a Late Bronze Age settlement (*Via Settevalli*) on the southern slopes of present-day Perugia (CECCARELLI L. & STODDART S. 2021; NEIL S. 2016). However, the settlements remained small and polyfocal in nature until the 7th century BCE, when the emerging city appears to gain a ritual focus, attested by the discovery of a deposition of a bucchero feasting vessels in the area underneath the modern cathedral (CECCARALLI L. & STODDART S. 2021). By the 6th century BC, the territory of Perugia seems to have been ruled by a small group of aristocrats, and during the later periods of this century the first cemeteries started to appear in the landscape surrounding Perugia (CECCARALLI L. & STODDART S. 2021). These elites appear to have been of local origin, as illustrated by the princely tomb at Castel San Mariano di Corciano, though there is also evidence to suggest that a small number of aristocrats might have migrated from Chiusi, as implied by the Sperandio Sarcophagus (late 6th - early 5th century BCE), which was likely imported from there (CECCARELLI L. & STODDART S. 2021). Big developments of the city seemed to have stagnated during the first half of the Classical period, as there is little to no 5th century activity in regard to the cemeteries surrounding Perugia, and the only evidence of the presence of monumental structures built during this time consists of two very fragmented architectural temple terracottas (CECCARELLI L. & STODDART S. 2021). However, by the time the 4th century rolled around, the city reawakened to become one of the most important Etruscan cities and managed to remain influential until the mid-1st century BCE (CECCERALLI L. & STODDART S. 2021). The fourth century saw the rise of large urban infrastructure, such as city walls, and an increase in cemeteries around Perugia (CECCERALLI L. & STODDART S. 2021; NEIL S. 2016). This trend of prosperity continued into the Hellenistic period, in which the city boasted even more large and monumental architecture with the completion of the city walls in travertine blocks, reaching a length of 3 kilometres, as well as 7 gates (two out of which still partially stand today), a travertine covered well (also still visible today)

and numerous iconic tombs, such as the tomb of the Volumnii and the tomb of Cai Cutu (Bizzarri R., Melelli L. & Cencetti C. 2018; Cecceralli L. & Stoddart S. 2021).

During this period cremation became the predominant funerary rite in the area of Perugia, a practise which continued into the Roman period (Ceccarelli L. & Stoddart S. 2021; Haynes S. 2000; Stoddart S. 2016b). However, a funerary custom typically found among the aristocratic families of Perugia included the inhumation of the founder of the tomb (*hypogeum*), with the later addition of the cremated remains of the (usually male) descendants in separate urns (Ceccarelli L. & Stoddart S. 2021). In some family tombs the number of accompanying cinerary urns reaches 50, as is the case in the Cai Cutu tomb (Cecceralli L. & Stoddart S. 2021).

Such urns come in different shapes and sizes and were mostly carved from travertine, but ceramic urns were occasionally used as well (Ceccarelli L. & Stoddart S. 2021; Haynes S. 2000). The urn's surface was likely covered with plaster, which was then brightly painted or even gilded at times, though sadly little of these surfaces remain (Haynes S. 2000). The most common type of urn from the late 4th century onward contains a lid shaped like a roof, with figure decorations depicting heraldic themes in its gables and sometimes a funerary banquet scene on the front (Haynes S. 2000). The appearance of a semirecumbent figure of the deceased on top of the lid is relatively rare in the case of Perugia, but they do occur from time to time between the end of the 3rd century and the first half of the 1st century BCE (Haynes S. 2000).

Although a lot of valuable materials seem to have been imported to Perugia through the centuries, workshops have been discovered where the cinerary urns were produced after models from Chiusi and Volterra, such as in the Satna workshop (Ceccarelli L. & Stoddart S. 2021). Iconographic types from these Etruscan cities were adopted and reinterpreted by Perugian artists, resulting in a local product (Ceccarelli L. & Stoddart S. 2021). The tombs themselves are commonly constructed using stone blocks, and have a rectangular plan, a ledge, benches and niches for the placement of urns, and a barrel-vaulted ceiling (Steingräber S. 2016). There are examples where the tombs contain barrel-vaulted side chambers as well, such as in the Ipogeo di San Manno (Steingräber S. 2016).

The reason the city of Perugia continued to flourish even after the defeat of the coalition of various Etruscan cities, Umbrians, Samnites and Gauls against Rome in 295 BCE (battle of Sentinum), is likely because the aristocratic families of Perugia sided with Rome during this conflict (Ceccarelli L. 2016; Ceccarelli L. & Stoddart S. 2021). This support appeared once again during the time of the Punic wars, when Scipio requested help to

carry the battle to Africa, and Perugia was one of the Etruscan cities to offer supplies (HAYNES S. 2000). However, the end of the city's importance is marked by its destruction by Octavius after the *Bellum Perusium* in 41-40 BCE, resulting in a full takeover of the territory by ever-expanding Rome (CECCARELLI L. & STODDART S. 2021).

2.3.1 Tomba dei Satna (Ponticello)

The first tomb to be discussed is the tomb ascribed to the aristocratic Satna family, discovered in 1968 at Ponticello di Campo, near Perugia (CENCIAIOLI L. & FERUGLIO A. E. 2004). Eight travertine cinerary urns were discovered inside the Hellenistic chamber tomb, representing 3 generations of the family, along with some grave goods that indicated that the tomb was likely in use between the middle of the 2nd century to the beginning of the 1st century BCE (CENCIAIOLI L. & FERUGLIO A. E. 2004). The rectangular structure was excavated from the rock, which is quite typical for contemporary tombs surrounding Perugia, and contained a stepped platform or bench along the back wall on which five out of the eight urns were placed; three on the higher step, likely the first to have been placed in the urn, and two on the lower step (CENCIAIOLI L. & FERUGLIO A. E. 2004). Two urns have been placed along the wall to the left of the entrance and one sits along the right wall (CENCIAIOLI L. & FERUGLIO A. E. 2004).

All of the urns were richly decorated and painted in vivid colours, depicting figurative scenes (in the case of urn 4 and 7 with a mythological theme) (CENCIAIOLI L. & FERUGLIO A. E. 2004). Furthermore, it seems that the ashes were wrapped in a cloth, possibly wool, and placed on top of another folded piece of textile that appear to be linen (CENCIAIOLI L. & FERUGLIO A. E. 2004). Mineralised samples of such textiles have been recovered from urn 2, 3, 4, 6 and 7, and it is interesting to note that these textiles are not the only thing that have been preserved due to mineralisation: The painted decorations on the surfaces of the urns have been sealed by calcium carbonate deposits, preventing further detachment and degradation (CENCIAIOLI L. & FERUGLIO A. E. 2004).

2.3.2 Tomb 27 (Strozzacapponi)

Just like Tomba dei Satna, tomb 27, is also a rectangular and subterranean type chamber tomb, dug out of the local travertine, dated to 2nd to 1st century BCE (GLEBA M., VANDEN BERGHE I. & CENCIAIOLI L. 2017). Tomb 27, as well as 29, are both part of the Strozzacapponi necropolis, which is located between the modern-day communes of Perugia and Corciano (GLEBA M., VANDEN BERGHE I. & CENCIAIOLI L. 2017). Travertine from this

region has been quarried since ancient times, and there are reasons to believe that the Strozzacapponi necropolis was the final resting place of the workers that were settled around the stone quarries they worked in, especially as most tombs seem relatively modest in decoration and burial goods (GLEBA M. & VANDEN BERGHE I. 2014; GLEBA M., VANDEN BERGHE I. & CENCIAIOLI L. 2017).

Just like the urns from Tomba dei Satna, the urn from tomb 27 was carved from travertine, however, aside from the name of the deceased, the rest of the urn was left undecorated (GLEBA M. & VANDEN BERGHE I. 2014). Urn 215166 located in tomb 27 contained heavily mineralised textile remains whose original structure could not be identified, and from which a sample was taken (GLEBA M. & VANDEN BERGHE I. 2014).

2.3.3 Tomb 29 (Strozzacapponi)

Also known as 'Tomba dei Letti Funebri', tomb 29 is the richest tomb of the Strozzacapponi necropolis, which is surprising when compared to the otherwise fairly modest tombs present at the rest of the site (GLEBA M. & VANDEN BERGHE I. 2014). Inscriptions let us know that the tomb has been used by the Anei Marcna family, a family possessing considerable amount of wealth as indicated by the richly decorated urns and impressive grave goods (GLEBA M. & VANDEN BERGHE I. 2014; GLEBA M., VANDEN BERGHE I. & CENCIAIOLI L. 2017).

Like the previously discussed tombs, tomb 29 can be dated to the 2nd and 1st century BCE, and is of a similar type, albeit more elaborate in its design due to the addition of a central pillar and a central recess (GLEBA M., VANDEN BERGHE I. & CENCIAIOLI L. 2017). Furthermore, benches ran along all three walls of the chamber, which was sealed off with a travertine block (GLEBA M., VANDEN BERGHE I. & CENCIAIOLI L. 2017). In total eight travertine cinerary urns were placed on top of the benches, each decorated with figurative reliefs and topped with a reclining figure representing the deceased painted in vivid polychrome (GLEBA M., VANDEN BERGHE I. & CENCIAIOLI L. 2017). Urn 5 contained multiple mineralised textile fragments, which were still partially purple in colour. Additionally, suspected traces of disintegrated textile were found on top. (GLEBA M., VANDEN BERGHE I. & CENCIAIOLI L. 2017). Both the textiles from the inside as well as on the outside of the urn were sampled.

CHAPTER 3:

Materials

Samples collected from Ponticello and Strozzacapponi came in numbered bags in their own system. These numbers correspond to the numbering of the Marie Curie project FIBRE (Fibre in Italy Before Roman Empire) conducted in 2009-2011 by Margarita Gleba, who collected the samples with permission of the appropriate institutions.

For the sake of this thesis these sample numbers were given a prefix in order to avoid confusion. The letter P or S signifies the cemetery the sample originates from (either Ponticello or Strozzacapponi). Some of these bags contained more than one fragment, in which case a letter would be added. These 'extra' sample numbers are mostly relevant for the work with the confocal laser scanning microscope; for the subsequent analyses they are considered to be the same sample as they are from the same context.

Not all of the samples gathered from these sites are textile samples, but instead some contain the soil associated with the textiles. These soil samples are not thoroughly studied in this thesis, since the focus is on the mineralisation of the textile. These soil samples are assigned numbers P04-30, P06-32, P10-37, and S05-42 and are listed in table 2.

Within this collection of samples, particularly among those from Strozzacapponi, are some that have been prepared for SEM analysis during previous studies of the samples. These samples consist of small carbon coated fragments on an SEM sample stub, and so are unsuitable for use in this study. Luckily, these prepared samples are sub-samples taken from S01-45 and S03-40, which are still present in an un-altered state within the sample collection. These previous studies were part of the FIBRE and DressID projects during which the textile parameters, original fibre and dyes of these samples were investigated. Various methods were used, such as optical microscopy, SEM, and HPLC-DAD. Furthermore, SEM-EDS was employed in order to identify the mineral components present on these samples. Results from these analyses have been incorporated in this chapter in order to provide a complete picture of these mineralised textile samples.

3.1 Sample list

Table 2 represents all of the samples within sample collection. A more extensive table can be found included within the appendix (table 14).

NO.	OLD NO.	COMBINED NO.	SITE	CONTEXT		MATERIAL
P01	23	**P01-23**	Ponticello	Tomba dei Satna	Urn 2	Textile
P02	27	**P02-27**	Ponticello	Tomba dei Satna	Urn 2	Textile
P03	29	**P03-29**	Ponticello	Tomba dei Satna	Urn 3	Textile
P04	30	**P04-30**	Ponticello	Tomba dei Satna	Urn 3	Soil
P05	31	**P05-31**	Ponticello	Tomba dei Satna	Urn 4	Textile
P06	32	**P06-32**	Ponticello	Tomba dei Satna	Urn 4	Soil
P07	33	**P07-33**	Ponticello	Tomba dei Satna	Urn 6	Textile
P07-B	33	**P07-33B**	Ponticello	Tomba dei Satna	Urn 6	Textile
P08	34	**P08-34**	Ponticello	Tomba dei Satna	Urn 6	Textile
P08-B	34	**P08-34B**	Ponticello	Tomba dei Satna	Urn 6	Textile
P09	36	**P09-36**	Ponticello	Tomba dei Satna	Urn 7	Textile
P10	37	**P10-37**	Ponticello	Tomba dei Satna	Urn 7	Soil
S01	45	**S01-45**	Strozzacapponi	Tomb 27	Urn 215166	Textile
S01-B	45	**S01-45B**	Strozzacapponi	Tomb 27	Urn 215166	Textile
S02	26	**S02-26**	Strozzacapponi	Tomb 27	Urn 215166	Textile*
S03	40	**S03-40**	Strozzacapponi	Tomb 29	'Sopra urna'	Textile
S04	25	**S04-25**	Strozzacapponi	Tomb 29	'Sopra urna'	Textile*
S05	42	**S05-42**	Strozzacapponi	Tomb 29	'Sopra urna'	Soil
S06	38	**S06-38**	Strozzacapponi	Tomb 29	Urn 5	Textile

Table 2: List of all the samples originating from Ponticello and Strozzacapponi (Perugia). Context of the samples are indicated by site, tomb, and urn number the samples were found in. Samples S03-40, S04-25 and S05-42 originate from outside one of the urns, as they are labelled '*sopra urna*' (above urn). The materials of the samples are also listed: The samples marked with an asterisk (*) have been altered during previous studies involving SEM analysis.

3.1.1 Ponticello - Urn 2

Urn 2 (figure 2) produced two samples with dissimilar appearances: P01-23 and P02-27 (figure 3). The former is a very small (approximately 4 x 2 mm) and fragile fragment, displaying an overall dark grey colour with white spots, while the latter is rather large (10 x 5 mm) and entirely white/ beige in colour (figure 3). Within the labelled bag of sample P01-23 (labelled '23') there is a SEM sample holder as well. This sample

Figure 2: Ponticello urn 2 pictured with its original content. Image provided by prof. M. Gleba.

holder does not have its own number, so it is not listed as a separate sample in the tables. Like the other SEM prepared samples, it is not used in this thesis.

3.1.2 Ponticello - Urn 3

Urn 3 (figure 4A) only produced one textile sample (P03-29) and a soil sample (P04-30). Sample P03-29 consists of one large fragment (10 x 4 mm) and a couple of small fragments. All pieces are white in colour (figure 4C).

3.1.3 Ponticello - Urn 4

Only one sample was recovered from urn 4 (figure 4B): Sample P05-31. This is a textile fragment of about 10 x 6 mm and has a white/ beige colour (figure 4D).

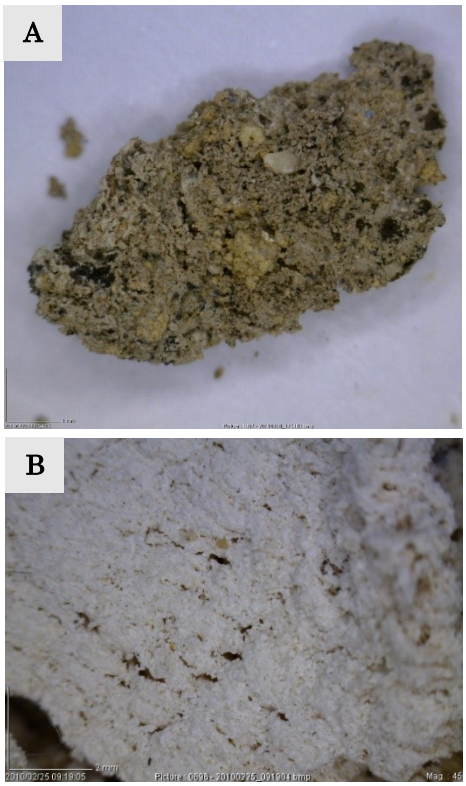

Figure 3: A: Sample P01-23 (20x) from Ponticello urn 2. **B:** Close-up of sample P02-27 (45x). Both images provided by prof. M. Gleba

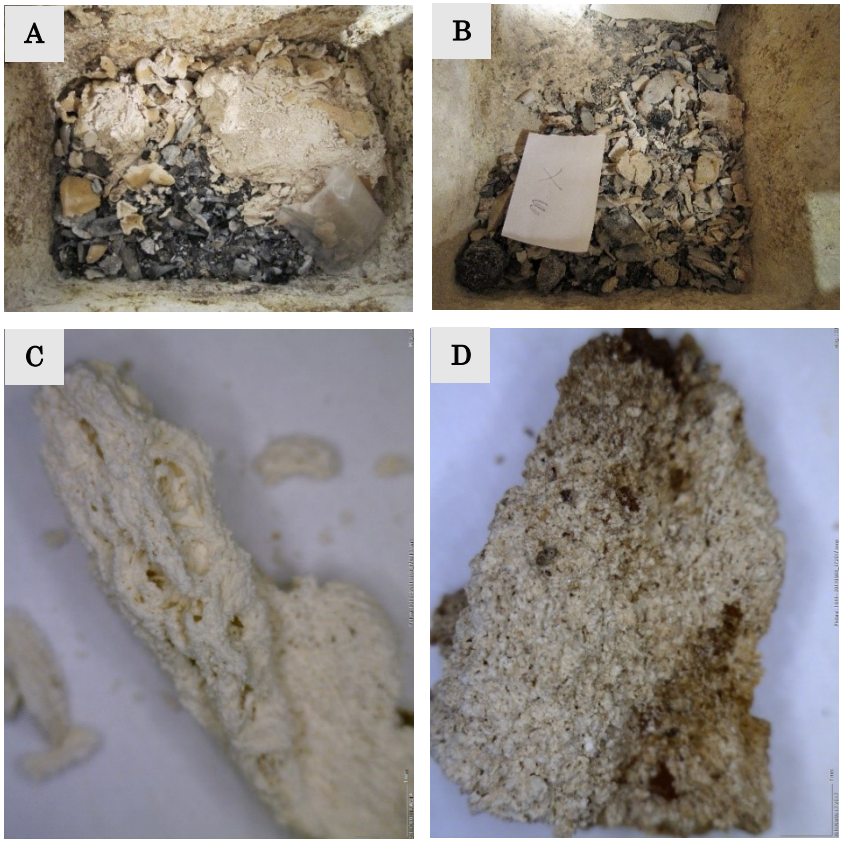

Figure 4: A: Urn 3 from Ponticello with its original contents. **B:** Ponticello urn 4 with its original content still present. **C:** Sample P03-29 (50x) from urn 3. **D:** Sample P05-31 (50x) originating from urn 4. All images provided by prof. M. Gleba.

3.1.4 Ponticello - Urn 6

Multiple samples originate from urn 6 (figure 5A), divided in two bags. The bag labelled 33 contains two large fragments (P07-33 and P07-33B) and an SEM sample holder. The SEM prepared sample is not used in this thesis. The smaller of the two fragments (6 x 4 mm) has been labelled B (P07-33B) for the work with the confocal laser scanning microscope, but it has a similar appearance to the large (9 x 4 mm) fragment. Both are white in colour. P07-33 is still somewhat recognizable as a textile fragment on first glance. The other bag labelled 34 contains two large brown fragments which are reasonably fragile. One of the fragments is slightly larger in size (10 x 7 mm) and is named P08-34. The smaller fragment (10 x 5 mm) has received the suffix 'B' for the CLSM analysis, becoming P08-34B. The brown colour and the reasonably fragile state of P08-34 and P08-34B might indicate that most of this sample has not fully mineralized.

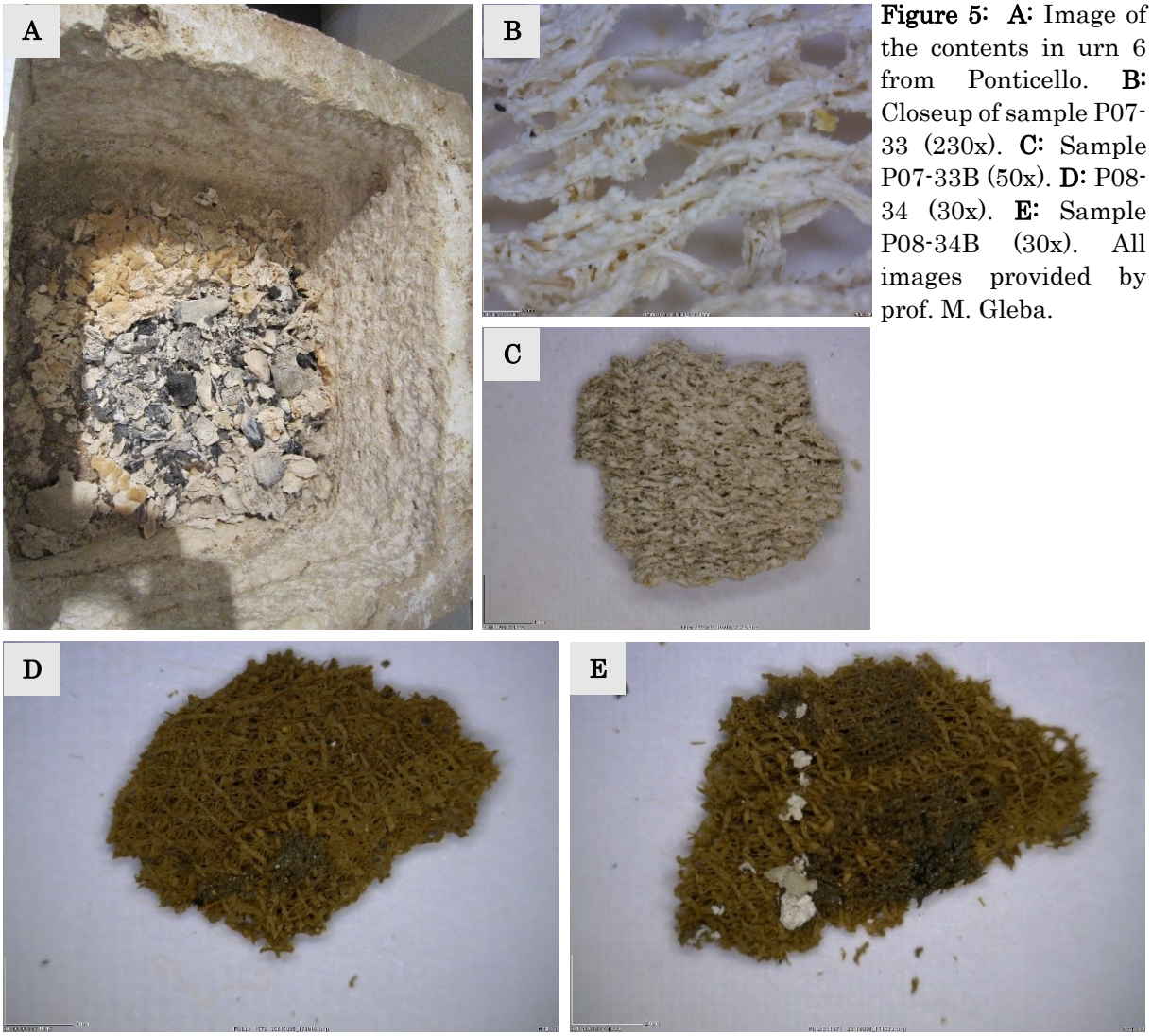

Figure 5: **A:** Image of the contents in urn 6 from Ponticello. **B:** Closeup of sample P07-33 (230x). **C:** Sample P07-33B (50x). **D:** P08-34 (30x). **E:** Sample P08-34B (30x). All images provided by prof. M. Gleba.

3.1.5 Ponticello - Urn 7

The last urn form Ponticello, urn 7, produced two samples, one of which is a soil sample and is not discussed further. The textile sample (P09-36, figure 6) recovered from this urn is rather large (20 x 16 mm), and like some of the previous samples is mainly white or beige.

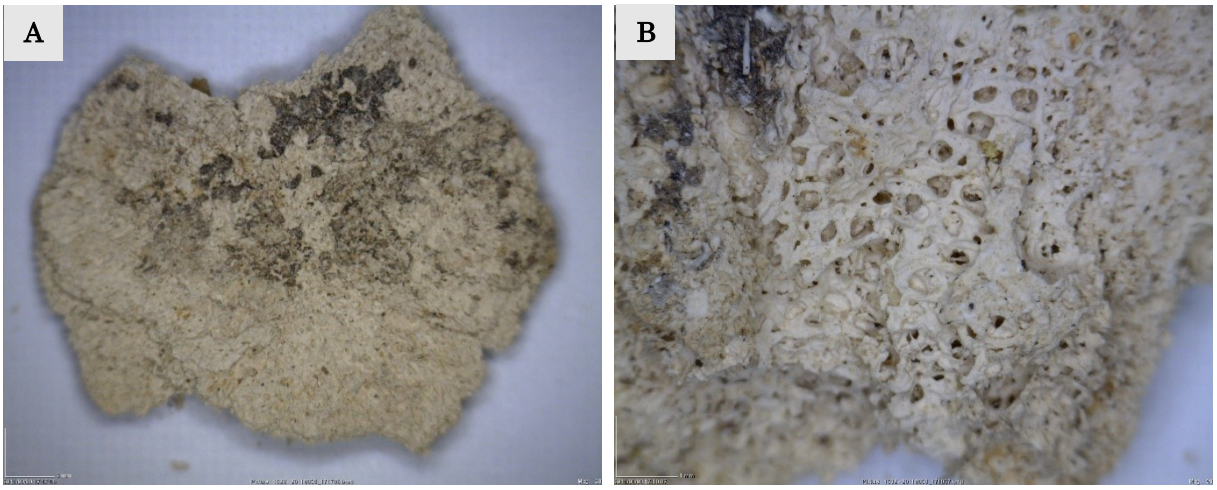

Figure 6: A: Sample P09-36 (20x) **B:** Close-up of sample P09-36 (50x). Both images are provided by prof. M. Gleba.

3.1.6 Strozzacapponi - Urn 215166

This urn has a rather peculiar number compared to the others. Two labelled samples exist for this urn: 45 and 26. Sample S02-26 consists of fragments prepared for SEM analysis and are attached to a SEM sample stub; these fragments were originally taken from 45. S01-45 consists of two main fragments, of which the smaller one (16 x 10 mm) received the 'B' suffix (S01-45B) for the CLSM analysis. S01-45 is quite large (20 x 15 mm) and is predominantly white in colour, as is the case for S01-45B (figure 7).

Figure 7: Mineralised textile fragments from urn 215166 before samples were taken from it. Image provided by prof. M. Gleba.

3.1.7 Strozzacapponi - Sopra urna

Multiple samples from Strozzacapponi have been labelled as '*sopra urna*' (above urn) (figure 8), of which one is a soil sample (S05-42), and another consists of multiple fragments on a SEM sample holder (S04-25). Sample S03-40 is a small textile fragment (10 x 7 mm) that displays a grey-ish brown colour. The fact that this fragment was not recovered from within one of the urns makes it an interesting sample to compare the other textile samples to, in order to see if there is a significant difference in mineralisation between the different contexts.

Figure 8: Full assemblage of textile fragments found *"Sopra Urna"* in tomb 29 of the Strozzacapponi necropolis. Sample S03-40 is a fragment of this collection. Interesting to note are the plant roots that are present in multiple fragments from this context. Image provided by prof. M. Gleba

3.1.8 Strozzacapponi - Urn 5

The final urn from Strozzacapponi from which a textile fragment has been recovered is urn number 5. This sample also includes a SEM stub with a fragment of sample S06-38. The rest of the sample consists of a fragment about 10 x 5 mm and displays a striking purple colour, which likely represents the textile's original colour (figure 9).

Figure 9: Image of sample S06-38 taken from Strozzacapponi urn 5. Image provided by prof. M. Gleba. Magnification 35x.

3.2 Textile technology

When it comes to archaeological textiles, different structural parameters can be used in order to identify used production techniques, cloth quality, and textile culture (GLEBA M. 2017b). Such parameters include thread diameter (in warp and weft), thread twist direction (in warp and weft), the type of textile weave, thread count per centimetre (in warp and weft), the material, and lastly, the presence of other diagnostic features and decorations (GLEBA M. 2017b).

Twist direction is commonly described by using the letters 'z' and 's', which represent a clockwise and counter-clockwise spin respectively, while 'i' is assigned to threads which do no display a discernible twist (figure 10) (GLEBA M. 2017b). Furthermore, the aforementioned terms 'warp' and 'weft' describe the two thread systems of a basic woven textile, where the static system kept in place by the loom is called the warp, and the moveable system passing between the warp threads is called the weft (GLEBA M. 2017a). There are various types of looms, but when discussing pre-Roman Italy, it seems that only vertical warp-weighted looms were used, until vertical two-beam looms eventually started to appear during the Roman Empire (GLEBA M. 2017a).

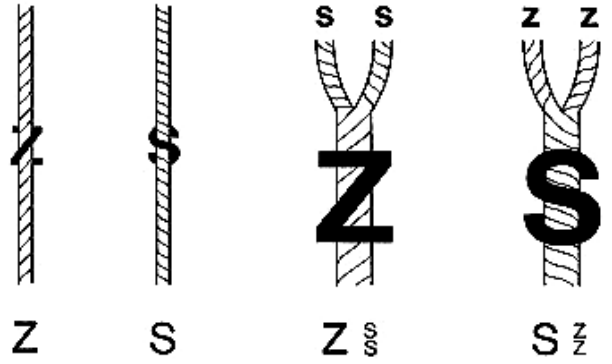

Figure 10: Twist directions of threads and their assigned letters. Image courtesy of BENDER JØRGENSEN L. 2004 (page 94)

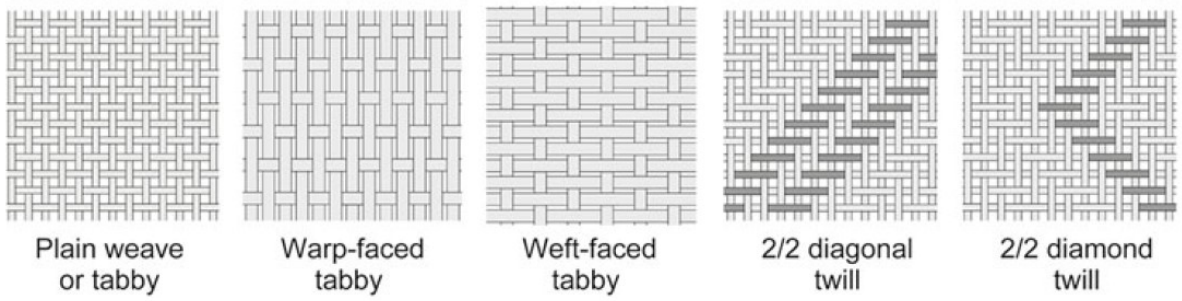

Figure 11: Common weave types found in Italy during the first millennium BCE. Image adapted from V. Herring & M. Gleba (GLEBA M. 2017b, 1207).

Aside from the continuous use of the vertical warp-weighted loom, numerous other characteristics of Italic textile culture have been recognized. Multiple weave types appear in the Italian archaeological record, and trends vary between regions (figure 11) (GLEBA M. 2017a). In general, a tabby weave is the most common type of weave found throughout Iron Age Italy, which is not all that surprising considering that this is the simplest weave technique on a loom, and can therefore be found in a multitude of places throughout prehistory (GLEBA M. 2017a; GLEBA M. 2017b). Balanced tabbies, which consist of approximately the same number of warp and weft threads alternating one over one, are commonly associated with funerary contexts in ancient Italy, where they have been used for shrouds or as wrapping material for grave goods (GLEBA M. 2017b). The threads of such tabbies are generally z-spun (clockwise), as are most threads used in Iron Age textiles in Italy (GLEBA M. 2017a). There is however an exception to this notion in the case of 2/2 twill weaves from the Italian peninsula; over half of Iron Age twills contain threads twisted in the opposite direction as well, creating a visual effect known as a spin or shadow pattern (GLEBA M. 2017a). In twill weaves the weft threads pass over and under the warp in a staggered pattern, creating various diagonal structures such as chevron, herringbone, diamond, broken diamond, cross, and plain diagonals (GLEBA M. 2017a). Furthermore, some of these Italic twills contain tablet woven borders (GLEBA M. 2017a). Tablet weaving is a complex and labour-intensive technique involving a (square) tablet with holes in its corners through which threads would be passed (GLEBA M. 2017a). Rotating these tablets in certain combinations would create narrow bands, suitable for belts, heading bands for a warp-weighted loom or decorative borders (GLEBA M. 2017a).

Aside from balanced tabbies and twills, warp-dominant and weft-faced tabbies appear in the Italian archaeological record as well (GLEBA M. 2017b). Warp-dominant tabbies, a type of tabby weave which has at least double the amount of warp threads per unit of length, are relatively rare (GLEBA M. 2017a). Interesting to note is that so far, all warp-dominant tabbies consist of plant fibre threads which are not draft spun (the dominant technique) but rather spliced, a technique that is most commonly associated with ancient Egypt and the Far East up until recently (GLEBA M. 2017a).

The opposite of warp-dominant are weft-faced tabbies, which, as one might have guessed, contain twice as many weft threads per unit of length compared to warp threads (GLEBA M. 2017b). This type of weave is fairly common, and the weft threads are often tightly packed to the point where the warp threads are no longer visible (GLEBA M. 2017a; GLEBA M. 2017b). Furthermore, another characteristic of this group of textiles worthy of note is

the lack of twist of the weft yarn, while the warp threads are strongly z-twisted (GLEBA M. 2017a; GLEBA M. 2017b).

Aside from weave type, a couple observations can be made regarding the materials of the textiles. In ancient Italy a wide array of materials was used, such as linen, hemp, esparto, tree bast, sheep wool, goat hair and even mineral asbestos (GLEBA M. 2016). Combining these with the observed weave types of the region the following trends become clear: Balanced tabbies most often appear to be made from plant fibres, where identification was possible, usually linen (GLEBA M. 2017a). This is also the case for warp-dominant weaves, as mentioned before (GLEBA M. 2017a). Twills, weft-faced tabbies, and tablet woven borders on the other hand are mostly, if not exclusively, produced from wool (GLEBA M. 2017a).

These are the overarching trends when it comes to the Iron Age textile culture, but let's not forget that regional variations exist, as the Italian Peninsula is a large area featuring ample cultural variation and various foreign influences. A good example that illustrates this are the imported Greek textiles and the later Greek-Italic hybrid productions that make their way, and eventually mostly take over, the indigenous traditions (GLEBA M. 2017a). The spin-patterned twills, balanced tabbies, and tablet woven bands from Italy share great similarities with textiles finds from Central Europe, down to the bronze button decorations (GLEBA M. 2017a; GLEBA M. 2017b). These production techniques were seemingly not practiced in ancient Greece, which appeared to follow an overarching Near Eastern textile tradition mainly consisting of fine (mostly woollen) weft-faced tabbies of high thread count (GLEBA M. 2017b). When contact between ancient Italy and Greece intensified from the sixth century BCE onwards, Italic textile culture seemed to shift toward a Greek model preferring the fine weft-faced tabby, especially in areas close to Greek settlements that were established on Italian shores (GLEBA M. 2017a; GLEBA M. 2017b). Eventually the weft-faced tabby became the preferred weave on most of the Peninsula, with only the northernmost border regions continuing the production of twills (GLEBA M. 2017b). However, the tablet woven borders appeared to remain important to the Italic population, as these were combined with the Greek style weave, creating a new and unique textile culture in Italy (GLEBA M. 2017b). This perfectly illustrates how studying textile production techniques can give insight into cultural developments.

During previous studies by Gleba & Vander Berghe (2014), the mineralised textile samples from Perugia were analysed on the basis of the aforementioned structural

Sample	Weave type	Twist (warp)	Twist (weft)	Threads/ cm (warp)	Threads/ cm (weft)	Diameter (warp)	Diameter (weft)
P01-23 *(Urn 2)*	n/a	-	-	-	-	-	-
P02-27 *(Urn 2)*	n/a	-	-	-	-	-	-
P03-29 *(Urn 3)*	Weft-faced tabby	z	i	10	n/a	-	-
P05-31 *(Urn 4)*	n/a	-	-	-	-	-	-
P07-33 *(Urn 6)*	Balanced tabby	-	z	17	20	0.1-0.2	0.2-0.3
P07-33B *(Urn 6)*	Weft-faced tabby	z	i	10	60-70	0.2-0.3	0.1-0.2
P08-34 *(Urn 6)*	Weft-faced tabby	z	i	20	60?	0.1-0.2	0.05-0.1
P09-36 *(Urn 7)*	n/a	-	-	-	-	-	-
S01-45 *(Urn 215166)*	n/a	-	-	-	-	-	-
S03-40 *('Sopra urna')*	n/a	-	-	-	-	-	-
S06-38 *(Urn 5)*	Balanced tabby	z	z	30-40	30-40	0.1-0.3	0.1-0.3

Table 3: Table adapted from previous research by Gleba M. & Vanden Berghe I. (2014).

parameters. In most cases the samples were too mineralised for proper identification of such features, however, it was possible to (partially) identify weave, twist, thread count

and diameter of the yarn, for samples P03-29, P07-33, P07-33B, P08-34 and S06-38 (see table 3). From this some interesting observations could be made, most notably the weft-faced tabbies from urn 6, which with their high thread count remind of the typical Greek textiles. Due to the degree of mineralisation the nature of fibre could not be identified during this 2014 study, which employed digital microscopy and a scanning electron microscope. However, other textiles from Italy boasting this type of weave (weft-faced, z-twisted weft threads, no discernible twist on the weft threads) have, where possible, only ever been identified as wool, so one can hypothesise that these textile fragments originally consisted of woollen yarn (GLEBA M. 2017a).

The fibres of the balanced tabbies within this sample collection have not been successfully identified either, though on the basis of previous patterns in the textile record from ancient Italy, one may assume that they were produced using a plant fibre. On the other hand, sample S06-38, the one which is of a pronounced purple colour, might be an exception to this assumption. This is because the dyeing of textile was usually done on woollen fabrics, while linen did not undergo the same practice and was usually left in its natural white colour (MARÍN-AGUILERA B., IACONO F. & GLEBA M. 2018).

Interestingly, dye analysis on the samples from Strozzacapponi during previous studies revealed that the still vibrant purple colour present on sample S06-38 is in fact, not the result of the prized shellfish-purple, but rather an 'imitation purple' possibly achieved with the use of lichen dyes (GLEBA M., VANDEN BERGHE I. & CENCIAIOLI L. 2017). However, during this same study it came to light that sample S01-45 actually did contain traces of shellfish purple, which is quite remarkable considering the relatively sober nature of the tomb (GLEBA M., VANDEN BERGHE I. & CENCIAIOLI L. 2017). The final sample from Strozzacapponi that was investigated in this way was sample S03-40, which was located on top of one of the urns in tomb 29. The chemical analysis indicated the presence of cinnabar, a valuable red pigment (GLEBA M., VANDEN BERGHE I. & CENCIAIOLI L. 2017). This pigment possibly has been transferred onto the textile through painted decorations of the urn, as cinnabar could have been used to paint important details on the urn (GLEBA M., VANDEN BERGHE I. & CENCIAIOLI L. 2017).

CHAPTER 4:

Methods

To get a good idea of the mineralization process that occurred on these textile samples, it is important to figure out which minerals are part of this process, as well as the state of the original organic material, if present at all: Are the fibres completely replaced or are they just encased in a mineral layer?

The first step comprises the investigation of the main overall features and characteristics of these samples, in order to observe the state of mineralisation and to get a better understanding of the state of the samples. The choice was made to perform this initial investigation using a confocal laser scanning microscope, which is able to obtain clear images of heavily textured samples with good magnification.

Then, using a portable Raman spectrometer an initial screening would be done to see what signals to expect from the samples and which next steps should be taken depending on the outcomes. A more precise benchtop Raman spectrometer can be used if there is a need for more precise measurements.

In the case of ample indications for organic materials during Raman spectroscopy, the use of FTIR-ATR was considered in order to get a clearer image of the organic compounds that might still be present within the samples. Lastly, to accurately identify the minerals present on the samples X-Ray diffraction would be performed in order to obtain crystallographic data, improving the identification of the mineral components.

4.1 Confocal laser scanning microscopy

For the initial analysis the choice was made to use a confocal laser scanning microscope (CLSM). This instrument uses laser light to produce high-resolution images of samples, by selectively illuminating only a specific focal plane of the sample, while also blocking out out-of-focus light from above and below that focal plane (SEMWOGERERE D., WEEKS E.R. 2005). It does this by using point illumination through a pinhole aperture, and in turn also allowing for only in-focus light to make back to the detector through the pinhole (NWANESHIUDU A., KUSCHAL C., SAKAMOTO F.H., ANDERSON R.R., SCHWARZENBERGER K., YOUNG R.C. 2012). To compensate for the loss of intensity of light by the pinhole technique, a stronger light source, such as a laser, is needed to obtain clear images (SEMWOGERERE D., WEEKS E.R. 2005).

There are two different variants of CLSM: Fluorescence-mode, mostly used in the field of biology, and reflectance-mode, used in this thesis (SEMWOGERERE D., WEEKS E.R. 2005). Reflectance-mode CLSM allows for extremely sharp and detailed images of heavily textured samples, a feat which is not possible with a conventional microscope (SEMWOGERERE D., WEEKS E.R. 2005; TENG X., LI F., LU C. 2020).
Another relevant advantage of reflectance CLSM is the ability to obtain colour images of the samples analysed. A different analysis technique commonly used to visualize the texture of a sample is scanning electron microscopy (SEM), however, because this technique uses an electron beam to map out the surface of the sample no information on the colour of the sample can be obtained (SCIAU P., GODET M. 2021).
Lastly, samples need little to no preparation before analysis with CLSM, keeping them in an unaltered state, allowing for a chemical analysis to be conducted on the same sample later without having to take surface alteration into account (TENG X., LI F., LU C. 2020).
All confocal images of the mineralized textiles were recorded in reflectance mode using an Olympus LEXT OLS4100 located at the Department of Geosciences of the University of Padua. This CLSM was equipped with five objectives (2.5x, 5x, 10x, 20x and 50x) and a 405nm laser. The image processing and compiling was done using the accompanying Olympus LEXT OLS4100 software package version 3.1.15.
To obtain a good overview of the samples' surfaces, the stitching application from the software was used to combine multiple individual images into a single one.

4.2 Raman spectroscopy

The CLSM analysis was followed by Raman spectroscopy, both portable and benchtop, in order to get a general idea of the general chemical composition of the samples on a molecular level. It is a fingerprinting technique that is excellent for identifying inorganic solids, but it can also be applied to a range of different materials, such as pigments (mineral, as well as organic and synthetic), waxes, varnishes, waxes, and plant fibres (SMITH G. D., CLARK R. J. 2004). Raman spectroscopy utilizes electromagnetic radiation in the form of monochromatic light, most often a laser (ROUSAKI A., VANDENABEELE P. 2021). When irradiating a sample, the molecules of said sample start to vibrate at higher frequencies, bringing the molecules to an excited vibrational state (ROUSAKI A., VANDENABEELE P. 2021). In agreement with quantum theory, molecules can only be excited to specific energy levels, as there are no transitional levels (ROUSAKI A., VANDENABEELE P. 2021). Most of the time this energy is immediately released, returning the molecule to its

ground state, during which the energy in the form of light is scattered (ROUSAKI A., VANDENABEELE P. 2021; SMITH G. D., CLARK R. J. 2004). This scattered light has the same energy level and wavelength as the inducing laser, and is called Rayleigh scattered light, which is a form of elastically scattered electromagnetic radiation (ROUSAKI A., VANDENABEELE P. 2021; SMITH G. D., CLARK R. J. 2004). This is, however, not all that occurs when irradiating a sample with monochromatic light. Not all of the molecules return to their ground level state; instead, a small portion of them end up in an energy level higher than their original state, resulting in the emittance of electromagnetic radiation with a difference in wavelength and energy level compared to the inducing laser and Rayleigh scattering, called Stokes scattering (ROUSAKI A., VANDENABEELE P. 2021). Stokes scattering can also occur when the excited molecules return to an energy state lower than its normal ground state, in which case the resulting scattering is known as anti-Stokes scattering (ROUSAKI A., VANDENABEELE P. 2021). Raman scattering includes both Stokes and anti-Stokes scattering, and by measuring the difference between the elastic scattering and the inelastic Raman scattering it is possible to study the molecular vibrations of the sample material (ROUSAKI A., VANDENABEELE P. 2021). It should be noted that anti-Stokes is significantly less intense than the Stokes counterpart, resulting in generally only the Stokes scattering being studied (ROUSAKI A., VANDENABEELE P. 2021). Another important measure is to filter out the Rayleigh scattering, as this type of scattering occurs much more often, to the point where it can completely drown out the Raman signal (ROUSAKI A., VANDENABEELE P. 2021).

This technique is generally considered to be non-destructive as long as careful attention is brought to the power of the laser in order to avoid thermal degradation or damage to the sample (ROUSAKI A., VANDENABEELE P. 2021). Other big advantages of the technique are that minimal to no sample treatment is needed, and both organic and inorganic components can be analysed, in crystalline as well as amorphous phases (ROUSAKI A., VANDENABEELE P. 2021).

However, potential problems can arise with the occurrence of fluorescence. This occurs when molecules are excited to an electronic state, resulting in a strong signal that drowns out the Raman scattering (ROUSAKI A., VANDENABEELE P. 2021). Short-wavelength lasers are much more likely to cause fluorescence, simply because they consist of a higher energy radiation level compared to long-wavelength lasers (ROUSAKI A., VANDENABEELE P. 2021). When opting for a low-wavelength laser in order to avoid fluorescence one must take the resulting lower Raman scattering possibilities and lower detector sensitivities into account (ROUSAKI A., VANDENABEELE P. 2021).

Raman spectrometers are usually coupled to an optical microscope, increasing the adaptability of the method, as it allows for a visual examination as well as a pinpointed analysis of a sample (SMITH G. D., CLARK R. J. 2004)

4.2.1 Portable Raman spectroscopy

Before moving on to Raman spectroscopy with a benchtop instrument a quick screening of the samples with a portable Raman spectroscopy device was done coupled with a microscope. Portable Raman spectrometer probes a larger surface area and contains a less sensitive detector than its benchtop counterpart. However, since it is coupled with a microscope it is possible to have a decent focus on the surface, allowing the acquirement of a spectrum for the area in focus (ROUSAKI A., VANDENABEELE P. 2021).
The portable Raman spectroscopy equipment was provided by the Department of Chemical Sciences of the University of Padua and consisted of a BWTEK inc. Raman spectrometer, with laser line at 785 nm, equipped with a BAC151 microscope. The spectra were recorded using the BWSpec software.

4.2.2 Benchtop Raman spectroscopy

After initial screening with a portable Raman spectrometer a second Raman analysis was performed with a benchtop Raman in order to obtain more precise results, as the benchtop system provides more stability and high-quality results, as well better spatial resolution as it is coupled with a more powerful microscope (ROUSAKI A., VANDENABEELE P. 2021). This technique was applied to samples for which clearer results were desired or which have small features that could not be properly analysed using the portable system.
This benchtop Raman spectrometer was located at the Department of Chemical Sciences of the University of Padua and consisted of an inVia Renishaw micro-Raman spectrometer, coupled with Leica Dm-LM microscope. The recording of the spectra was done using the Renishaw Wire 4.4 software.
During this analysis 514 nm laser was used, which is potentially a source of increased fluorescence, but it can probe the inorganic fraction with more precision. As the primary goal of this step was to identify the minerals previously observed using the CLSM, this limitation was not expected to cause an issue for this analysis. Furthermore, the use of lasers with different wavelength is recommended in Raman, because some compounds could give poor Raman signals at a specific wavelength and very good signals at another

wavelength. Different laser power and optical magnifications were used to acquire the Raman spectra.

4.3 FTIR-ATR spectroscopy

To get a better understanding of the organic components that could possibly be present within the mineralised samples, FTIR-ATR analysis was performed on small fragments of the samples, as Raman spectroscopy can have some trouble identifying organic components due to the fluorescence effect it can cause, overwhelming the Raman signal.
FTIR-ATR spectroscopy is also a vibrational technique like Raman spectroscopy; however, it utilizes infrared radiation instead of monochromatic light (ROUSAKI A., VANDENABEELE P. 2021). Functional groups can be identified by using their characteristic vibrational frequencies in the IR region, which can yield both chemical and structural information on both organic and inorganic materials (LIU G.L., KAZARIAN S. G. 2022). When dealing with cultural heritage materials the mid-IR range (4000-400 cm^{-1}) is often used, as most of the organic and inorganic materials usually associated with cultural heritage can be found within this range (LIU G.L., KAZARIAN S.G. 2022).
There are different modes FTIR spectroscopy can be performed in, and during this research ATR was selected. This is because ATR requires very little sample preparation, if any, and can quickly produce consistent results (GRIFFITHS P.R., DE HASETH J.A. 2007). During this technique the sample is placed in contact with a sensing element with a high refractive index (Internal Reflection Element: IRE); in this case diamond was used as IRE (GRIFFITHS P.R., DE HASETH, J.A. 2007; LIU G.L., KAZARIAN S.G. 2022). IR radiation is not directly transmitted through the sample, rather, an IR beam is directed through the IRE at its critical angle causing total internal reflection to occur (GRIFFITHS P.R., DE HASETH, J.A. 2007; LIU G.L., KAZARIAN S.G. 2022). This standing wave of radiation within the IRE interacts with the sample that is in contact with it, absorbing part of the IR beam (LIU G.L., KAZARIAN S.G. 2022). The IR beam which is now weakened through the interaction with the sample exits the IRE and reaches the detector where the signal is converted to an absorbance spectrum (LIU G.L., KAZARIAN S.G. 2022).
To ensure adequate contact between the sample and the IRE, small fragments needed to be firmly pressed against it, essentially crushing a small part of the sample. This makes this analysis technique micro-destructive. The crushed fragments have been recovered in their fragmented state and are still part of the sample assemblage. Since no other

alterations are necessary in order to analyse the samples with FTIR-ATR, these retrieved fragments could still be used for chemical analysis in the future.
The FTIR-ATR analysis of the samples was made using a Bruker Optics mod. Alpa T FTIR spectrometer equipped with a Broker Optics platinum ATR QuickSnap™ module and a diamond ATR plate, located at the *Centro di Analisi e Servizi Per la Certificazione* (CEASC) in Padova. All spectra were acquired with 32 scans, ATR-corrected. All the samples were acquired. The spectral data was recorded using Bruker Opus software, after which it was analysed further using Microcal Origin Pro 2022b analytical software.

4.5 X-ray diffraction

In order to obtain more conclusive results in regard to the inorganic components of the samples, the choice was made to perform XRD analysis as a final step. Due to some time constraints and because some samples showed very similar results thus far, a selection was made. The samples chosen for this last type of analysis were selected based on their visual group (at least 1 sample from every group, identified during the CLSM analysis), as well as previous interesting results (identification of more than one component, or the possible presence of organics). These criteria resulted in the selection of samples P01-23, P03-29, P07-33, P09-36, S03-40, and S06-38
XRD is a technique that is mainly applied to study crystalline solids, as it is able to determine the crystalline structures of the probed material, though it can also be used to study a variety of other substances (DOWSETT M., WIESINGER R. & ADRIAENS M., 2021). It is most useful in combination with analysis techniques that determine the elemental composition of a material, especially when the probed sample consists of a mixture of materials (which is most often the case when dealing with cultural heritage materials), as knowledge of the elements present in a sample aids in interpreting complex XRD data, resulting in identification of the specific compounds present (DOWSETT M., WIESINGER R. & ADRIAENS M., 2021).
XRD uses the relationship between the wavelength of X-rays (± 0.25 - 0.05 nm) and the spacing between atoms in a crystalline material (which is similar to the wavelength of X-rays) (DOWSETT M., WIESINGER R. & ADRIAENS M., 2021). When the incident X-ray beam hits the planes of atoms in a crystalline material intense X-ray peaks can be detected (*diffraction peaks)*. These diffraction peaks occur at certain angles with respect to the incident beam, forming a distinct pattern of peaks for different crystal structures (DOWSETT M., WIESINGER R. & ADRIAENS M., 2021). This phenomenon is however not a reflection of

the incident X-rays, in which case the intensity would remain the same. Instead, the X-rays excite the electrons of the atoms within the crystalline structure to a heightened energy level (REF). This heightened energy level cannot be maintained, thus the energy is released and scattered (REF). This scattering can occur in two ways, one in which the released energy is of the same wavelength as the incident X-rays (*coherent scattering*), or conversely, the scattered energy has changed compared to the incident one (*incoherent scattering* or *Compton scattering*) (DOWSETT M., WIESINGER R. & ADRIAENS M., 2021). It is this coherent scattering that contributes to the diffraction pattern, as incoherent scattering only contributes background signal (DOWSETT M., WIESINGER R. & ADRIAENS M., 2021). The coherent scattered X-rays interfere with each other: At certain angles of the incident beam, the wavelength of the X-rays equals the distance between the atoms in the crystal, scattering these rays in phase (DOWSETT M., WIESINGER R. & ADRIAENS M., 2021). This means that their path lengths are the same or differ a whole number of wavelengths, amplifying each other, and thus increasing the intensity (Cullity D.B., Stock S. R. 1956). Using Bragg's law ($\lambda = 2d \sin \theta$), it is possible to calculate the distance between atoms using the angle where diffraction occurs, thus identifying the geometry of the probed crystal (Cullity D.B., Stock S. R. 1956; DOWSETT M., WIESINGER R. & ADRIAENS M., 2021). Such calculations and the acquisition of diffraction patterns from XRD data can be relatively easily obtained using powerful software, such as HighScore in this case, where combined with databases containing reference patterns it is possible to identify the compounds of the probed sample (DOWSETT M., WIESINGER R. & ADRIAENS M., 2021). The XRD analysis on the selected mineralised textile samples was done using a PANanlytical X'Pert PRO diffractometer with Bragg Brentano geometry in transmission focusing mode through a dedicated mirror, Cu K-alpha radiation, PIXcel detector and a reflection-transmission spinner sample stage, located at the Department of Geosciences of the University of Padua. The collected data was then interpreted using HighScore version 5.2.

CHAPTER 5:

Results

5.1 Confocal laser scanning microscopy

After analysing all of the samples using CLSM, they were divided into four groups based on their visual characteristics (table 4 and figure 12).

Group 1 only contains three samples, of which two originate from the same urn (samples P01-23 and P02-27), and the other, sample S03-40, is the lone sample that was discovered outside of one of the urns (labelled "sopra urna", meaning 'above urn'). This group's main characteristic is the overall more chaotic mix between light and darker – almost black – minerals, and an almost complete absence of any textile structure.

The second group (group 2) is quite similar to group 1, but there is one main difference: The darker minerals present on these samples are more clustered together and overall display more brown-ish colour to them compared to the dark minerals found on the samples assigned to group 1. Additionally, like the previous group, the original textile structure seems to be absent, however the samples originating from Strozzacapponi within this group (S01-45 and S01-45B) display some lattice like patterns of dark brown minerals that could have possible originated from the textile's original weave pattern.

The most striking feature of the third group (group 3) is the near-complete coverage of the samples by tiny white crystals, with only limited intermingling of other materials. More interestingly, these samples still display the original texture of the textile (albeit to varying degrees).

Lastly, group 4, perhaps most remarkable in appearance, contains samples that might still display some degree of their original colour (samples displaying a purple, pink-ish, or faded orange tone). Additionally, another significant feature of this group is the fact that the original textile structure is still very clearly recognizable. Interesting to note is that two samples that are a part of this group (P08-34 and P08-34B) share their context with two samples that are distributed to group 3 instead (P07-33 and P07-33B): These samples all originated from urn 6 from Tomba dei Satna (Ponticello) but do not share the same main features. However, all four of these samples show the original textile structure, though there is a significant difference between the samples from group 3 and 4. Still, all samples originating from urn 6 are seemingly in a relatively better state of preservation compared to most of the other urns.

Group	*Description*
1	Overall ashy colour caused by a mix of light-coloured and dark grey & black areas. Textile structure as good as absent.
2	Mostly covered by white & light-coloured crystals, with darker areas that are usually brown in colour. Textile structure as good as absent.
3	Almost completely covered in white crystals. Textile structure still visible or implied.
4	Purple, pink-ish or faded orange in colour, possibly reflecting the fibres' original colour. Textile structure still fully visible.

Table 4: Table containing the visual groups and their description, based on images obtained from CLSM.

Figure 12: Images taken with the CLSM illustrating the different visual groups. All images were taken by the author. **A:** Image of sample P01-23 at magnification 10x. Sample P01-23 represents visual group 1. **B:** Image of sample P09-36 at magnification 5x, representing visual group 2. **C:** Image of sample P07-33 at magnification 5x, assigned to visual group 3. **D:** Image of sample S06-38 at magnification 10x. Sample S06-38 represents visual group 4.

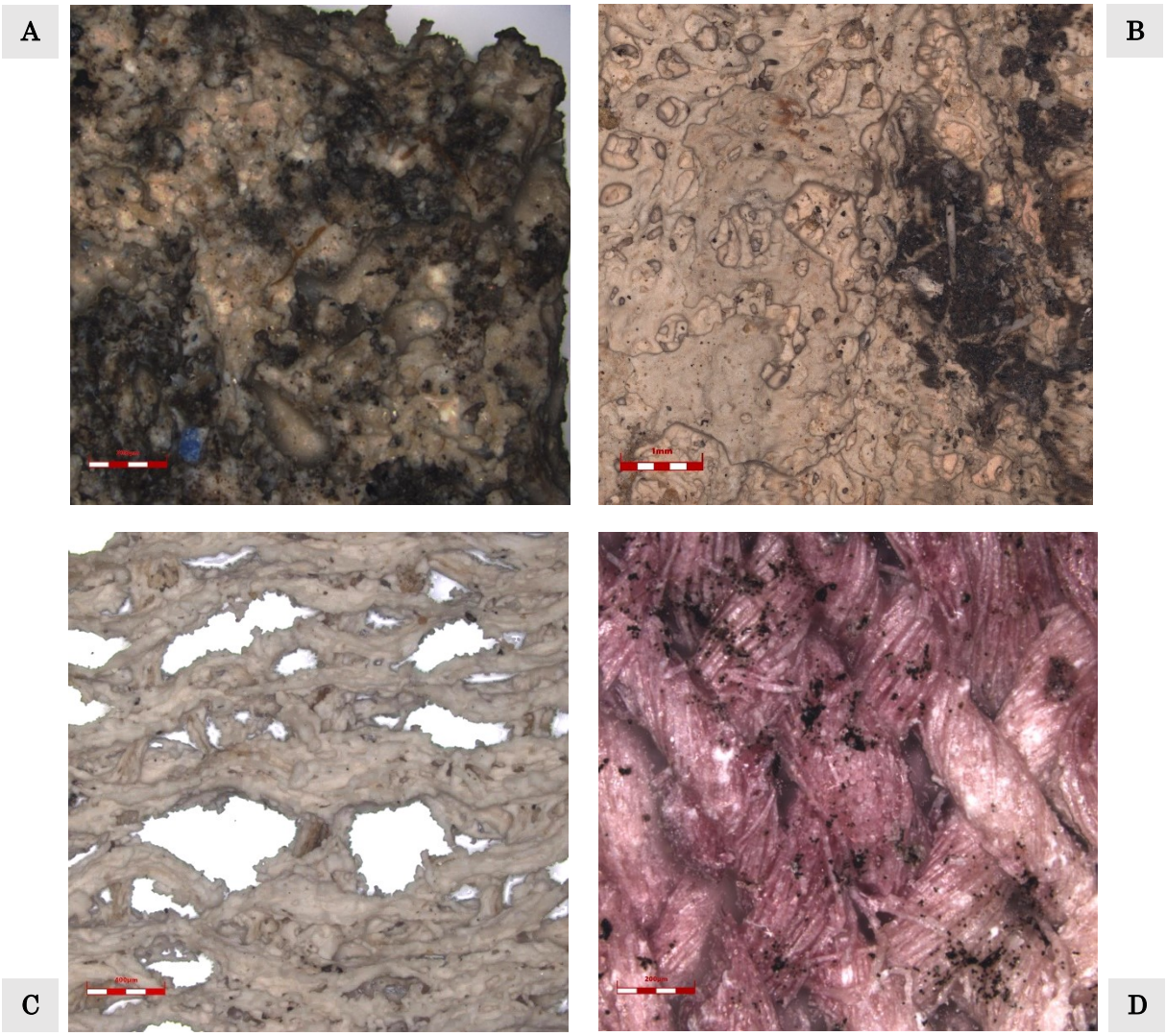

Category	Description
1	Original organic material of the textile fibres is still present (on the surface).
2	Original organic material of the textile fibres is encased in minerals, but the original textile texture is possibly still present.
3	Original material of the textile fibres is mineralized to the point that it is no longer clearly recognizable as a textile.

Table 5: Table describing the different categories of the possible mineralization state of the samples.

Instead of these four groups, it is also reasonable to assign the samples just to two groups: One group containing samples predominantly covered by light coloured minerals (groups 1,2 and 3), and another containing the samples that still mostly resemble their original colour and structure (group 4).

One of the main purposes of conducting this analysis was to locate areas of interest, specifically areas that display different levels of mineralization, to then be subjected to micro-Raman analysis. For this reason, 3 categories were identified: 1, the original material of the textile is still present (to some degree), 2, the original texture and structure of the textile is still visible, but the fibres are completely encased by minerals, and 3, the original material has been mineralized to the degree that the original texture is (almost) no longer visible (Table 5). However, it turned out that hardly any sample displayed clear and indisputable areas where the original organic material might still be present. There are some spots here and there that could perhaps be eligible for micro-Raman analysis as a potential organic fibre, but it might not yield the desired results as it is not certain if organic matter is still there. Even though organic fibres might not be present on the surface any longer, other unexpected features came to light during the CLSM analysis. No less than four out of thirteen samples contained at least one bright blue mineral (Figure 14). Both samples from Ponticello urn 2 (P01-23 and P02-27) contain it, as well as two out of the four samples collected from Strozzacapponi (S01-45 and S03-40). Interestingly, other samples taken from the Strozzacapponi necropolis contain colourful features as well. Aside from the aforementioned blue minerals, sample S03-40 contains some type of orange mineral and some green areas, while purple areas can be observed on sample S01-45B and S06-38 (S06-38 is mostly purple actually) (figure 15). Furthermore, two samples (P08-43 and S03-40) contain features that resemble insect shell embedded in between the minerals (figure 13). For sample S03-40 this might be less surprising as this sample was retrieved outside of the urn.

P O N T I C E L L O (Perugia)				
Context		*Sample*	*Visual group*	*Mineralization state*
Tomba dei Satna	**Urn 2**	P01-23	1	3
		P02-27	1	3
	Urn 3	P03-29	3	3
	Urn 4	P05-31	2	3
	Urn 6	P07-33	3	2
		P07-33B	3	3
		P08-34	4	2
		P08-34B	4	2
	Urn 7	P09-36	2	3
S T R O Z Z A C A P P O N I (Perugia)				
context		*Sample*	*Visual group*	*Mineralization state*
Tomb 27	**Urn 215166**	S01-45	2	3
		S01-45B	2	3
	'Sopra urna'	S03-40	1	3
Tomb 29	**Urn 5**	S06-38	4	2

Table 6: Table containing an overview of the samples and their classification in relation to their visual groups and mineralization state, as well as their context.

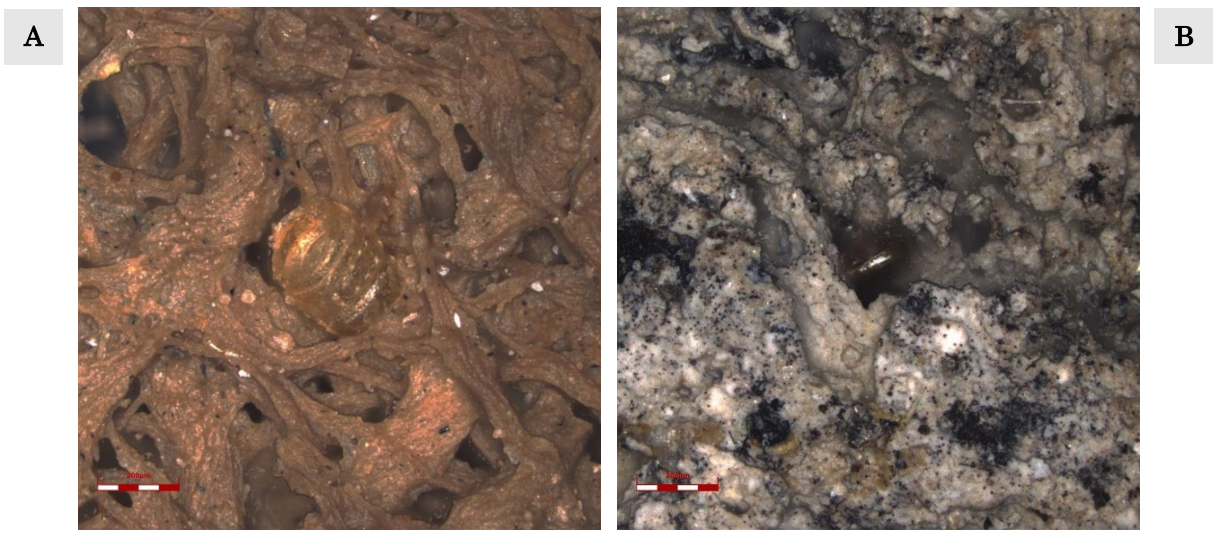

Figure 13: CLSM images taken by author showing features that resemble insect shells embedded within the samples. **A:** Sample P08-34, magnification 10x. **B:** S03-40, magnification 10x.

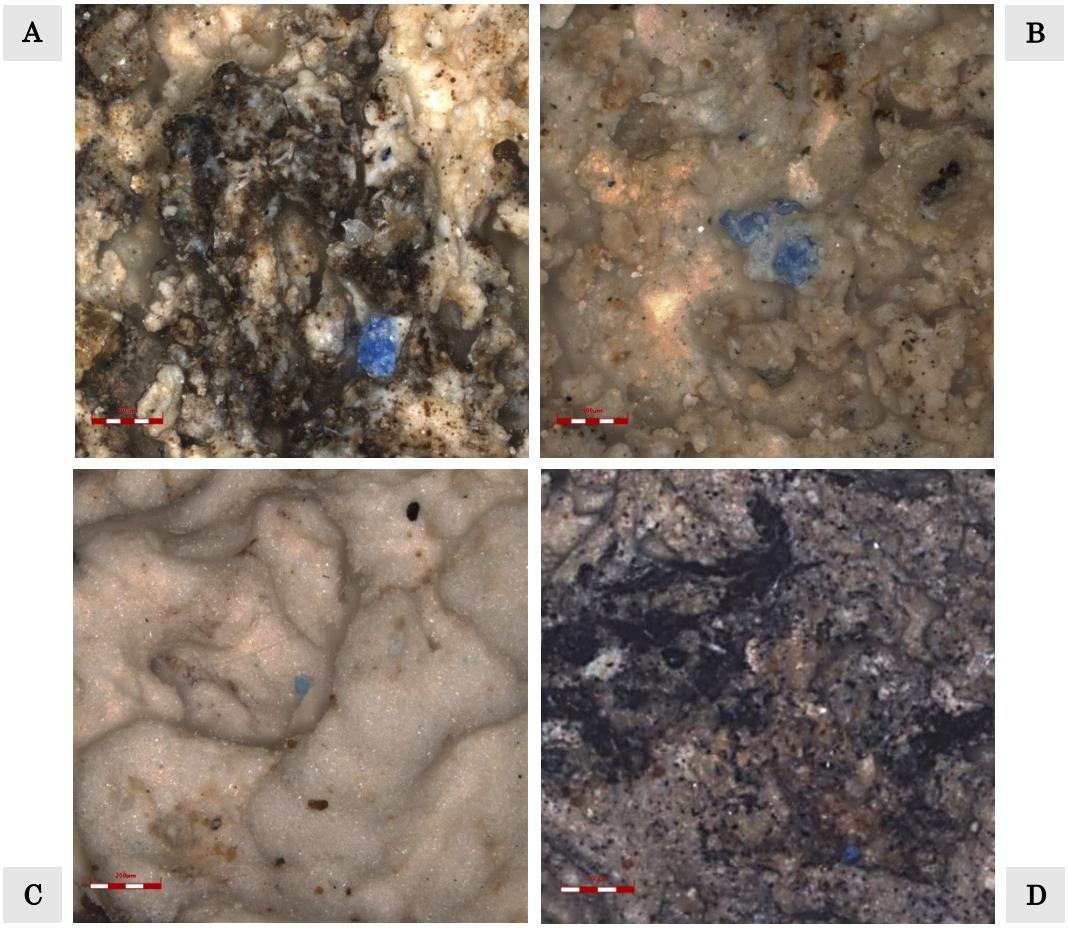

Figure 14: CLSM images showing the blue minerals discovered on multiple samples. All images were taken by the author. **A:** Sample P01-23, magnification 20x. **B:** Sample P02-27, magnification 20x. **C:** Sample S01-45, magnification 10x. **D:** Sample S03-40, magnification 5x.

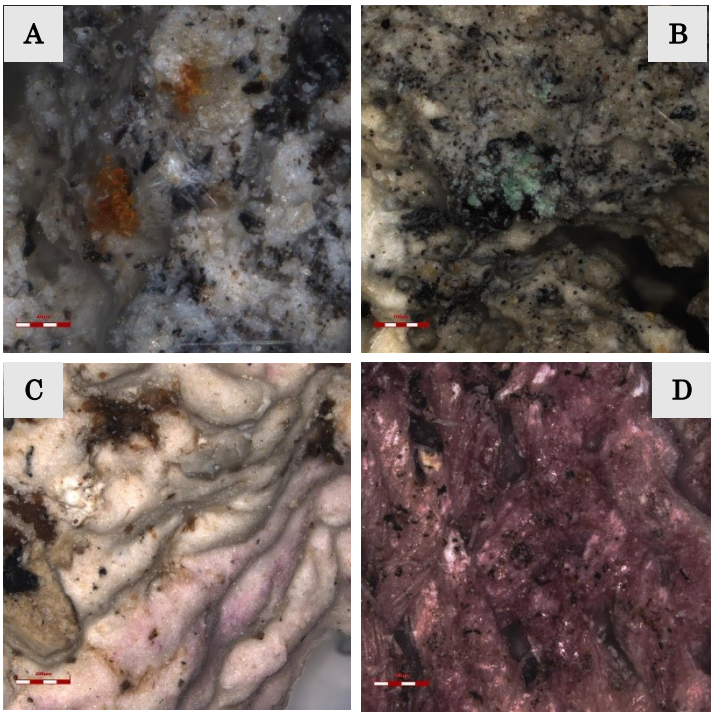

Figure 15: CLSM images showing different coloured features observed on various samples. All images were taken by the author. **A:** Sample S03-40, magnification 50x, showing orange-coloured spots. **B:** Sample S03-40, magnification 20x, a faint green colour can be observed on the surface of the sample. **C:** S01-45B, magnification 10x, sample shows a faint purple spot on the surface of the sample. **D:** Sample S06-38, magnification 10x. This sample is almost completely purple, and seems different from the purple area on sample S01-45B, which only faintly appears on the surface.

5.2 Raman spectroscopy

5.2.1 Portable Raman spectroscopy

For most of the samples no clear Raman signal could be observed due to a strong fluorescence effect. For samples P03-29, P07-33, S01-45, and S06-38 a Raman spectrum could be retrieved from the white parts of the samples (figure 16). Interestingly, one of these four samples displayed a different result compared to the other three. Sample S06-38 had an observable signal for calcite (main identifying peaks at 446 cm^{-1}, 490 cm^{-1}, and 1083 cm^{-1}). The other samples that yielded results had signals for gypsum instead, identifiable by a big peak at 1006 cm^{-1} and smaller peaks around 480-490 cm^{-1}. However,

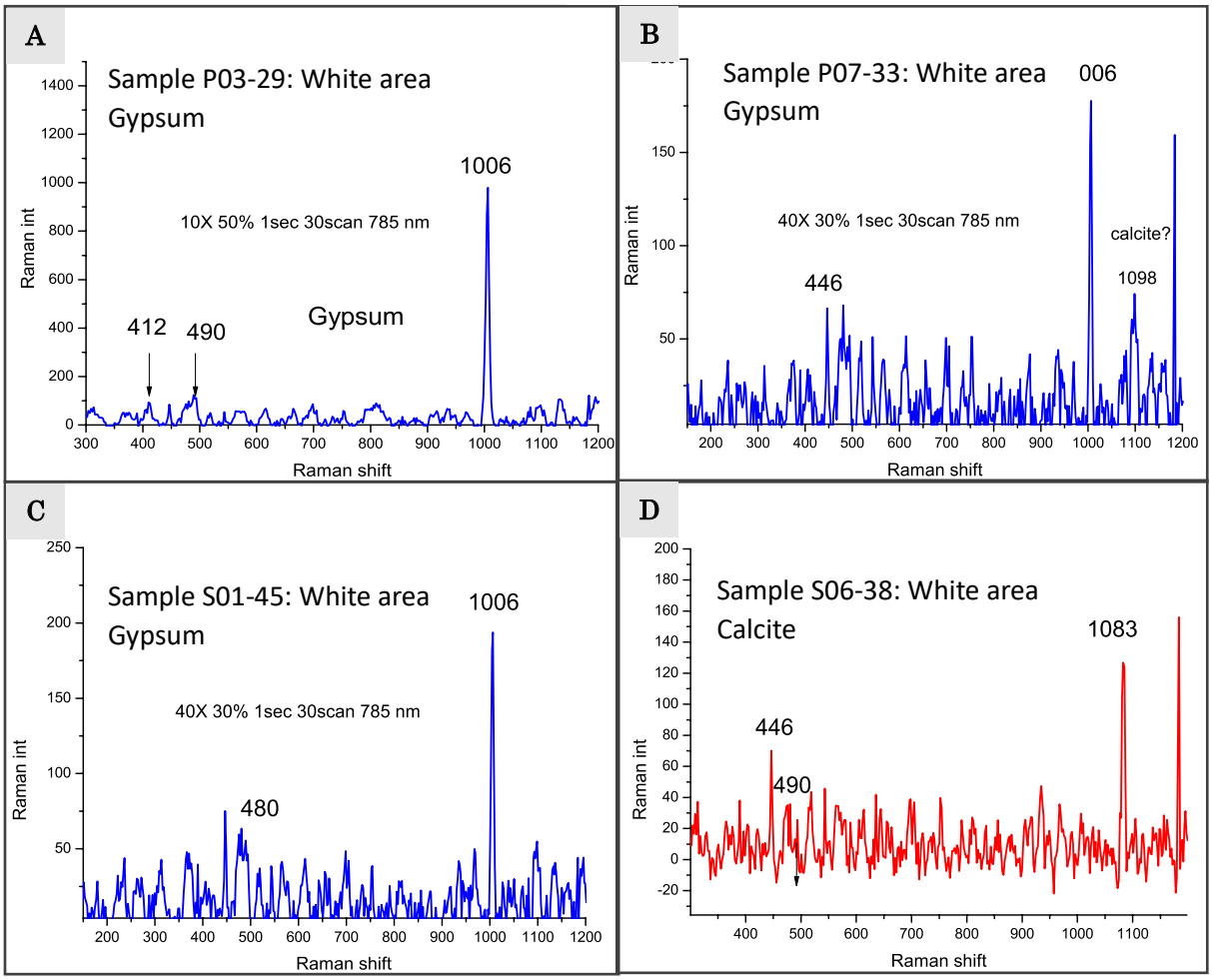

Figure 16: Raman spectra that have been acquired using the portable Raman spectrometer, with the help of prof. A. Zoleo of the Department of Chemical Sciences of the University of Padua. **A:** Raman spectrum of a white area of sample P03-29, displaying a signal for gypsum. **B:** Raman spectrum of a white area of sample P07-33, showing peaks for gypsum, but there is a possible weak calcite signal as well. **C:** Raman spectrum of a white area of sample S01-45 indicating the presence of gypsum. **D:** Raman spectrum of a white area of sample S06-38, which is the only sample with a clear indication of the presence of calcite so far.

sample P07-33 could potentially also contain some calcite, as indicated by a peak around 1098 cm^{-1}.

Attempts were made to analyse the darker minerals and the coloured areas localized during the CLSM analysis, however due to the lack of precision of the instrument they were very difficult to localize. When it was possible to localize such areas, such as the blue minerals discussed in the previous section, the strong fluorescence effect drowned out any useful Raman signal.

Sample	*Raman signal (portable)*
P01-23	n/a
P02-27	n/a
P03-29	Gypsum
P05-31	n/a
P07-33	Gypsum (+ weak calcite signal?)
P08-34	n/a
P09-36	n/a
S01-45	Gypsum
S03-40	n/a
S06-38	Calcite

Table 7: Overview of the portable Raman results, showcasing that the majority of the analysed samples did not yield useable spectra. Gypsum appears most often in the small group of samples where spectra could be obtained.

5.2.2 Benchtop Raman spectroscopy

Since the results of the portable Raman spectroscopy were not as useful as expected, the choice was made to try again for all of the samples with the benchtop setup. Unfortunately, fluorescence caused too much interference for half of the samples, and thus no readable Raman spectrum could be obtained. However, at least one useable spectrum could be obtained for samples P01-23, P03-29, P07-33, S03-40, and S01-45 (though multiple areas of the samples were probed).

Sample P01-23 was previously ascribed to visual group 1 due to its mix of darker/ grey and white areas. Both areas were probed, but only the white area resulted in a spectrum: The typical peaks of gypsum (1010 cm^{-1}, 416 cm^{-1} and 625 cm^{-1}) (figure 17).

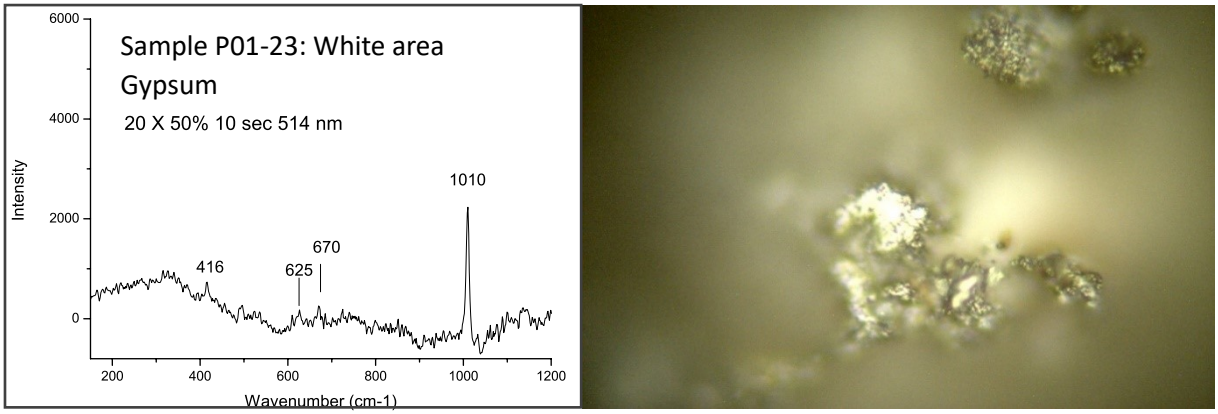

Figure 17: Raman spectrum of the white area of sample P01-23 (left) and image of the probed area at magnification 20 (right). Raman spectrum has been acquired using the benchtop Raman spectrometer, with the help of prof. A. Zoleo of the Department of Chemical Sciences of the University of Padua.

A similar situation, where only the white areas yielded a readable spectrum, occurred for samples P03-29, P07-33, and S01-45. Following the results of the portable Raman, both of these spectra indicated the presence of gypsum, as shown by the main peak around 1010 cm^{-1} (figure 18).

Unlike the previous four samples, sample S03-40 is the only sample where a readable spectrum could be acquired from one of its black areas instead. This spectrum resulted in a pattern that could be attributed to carbon black (figure 19).

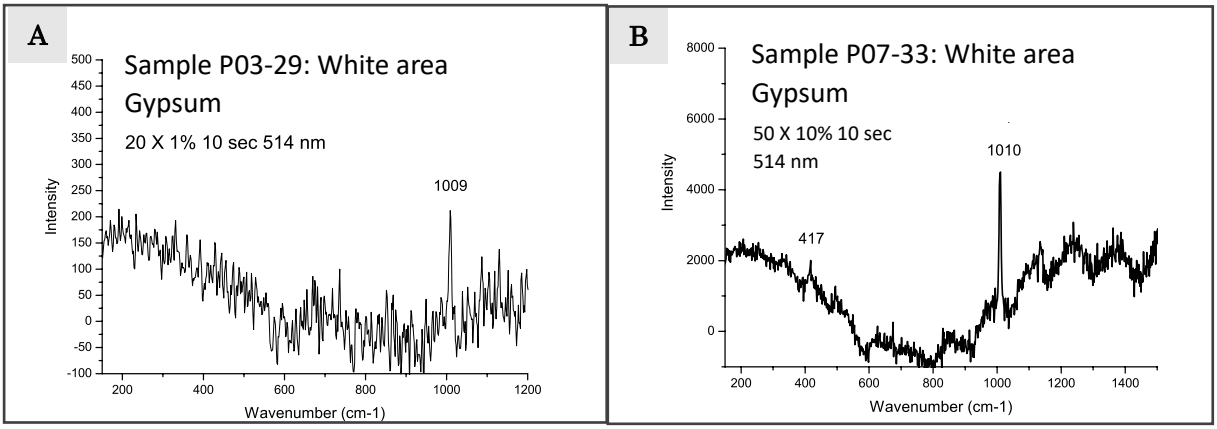

Figure 18: Raman spectra samples P03-29 (**A**) P07-33 (**B**). Both samples were mostly covered in white minerals. Raman spectra have been acquired using the benchtop Raman spectrometer, with the help of prof. A. Zoleo of the Department of Chemical Sciences of the University of Padua.

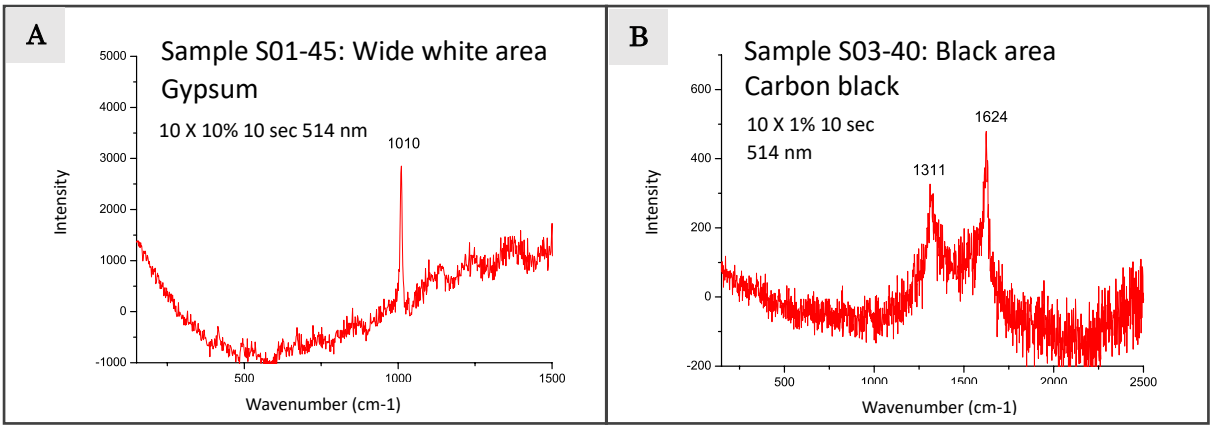

Figure 19: Raman spectra samples S01-45 (**A**) and S03-29 (**B**). Raman spectra have been acquired using the benchtop Raman spectrometer, with the help of prof. A. Zoleo of the Department of Chemical Sciences of the University of Padua.

Sample	*Raman signal (benchtop)*
P01-23	Gypsum
P02-27	n/a
P03-29	Gypsum
P05-31	n/a
P07-33	Gypsum
P08-34	n/a
P09-36	n/a
S01-45	n/a
S03-40	Carbon black
S06-38	Gypsum

Table 8: Overview of the benchtop Raman results, showcasing that the majority of the analysed samples did not yield useable spectra. Gypsum appears most often in the small group of samples where spectra could be obtained.

5.3 FTIR-ATR spectroscopy

Due to the Raman analyses not producing clear results for the majority of the samples, all the samples were subjected to FTIR-ATR analysis. The spectra obtained with FTIR-ATR spectroscopy are mostly consistent with the results acquired during the portable Raman analysis. There are some minor exceptions however: In the results of the portable Raman of sample P07-33 showed a possible, but very weak, signal for calcite. This signal did not resurface in the FTIR-ATR analysis, as only a signal for a dehydrated form of gypsum

could be identified. Interestingly, sample S06-38 displayed a similar situation, albeit in reverse: During the portable Raman analysis a signal for just calcite could be identified, while a weak signal for gypsum could be observed in the IR spectrum. Furthermore, the calcite pattern seems to be shifted a little to the left (main peak of calcite for sample S06-38 is at 1395 cm^{-1} instead of the usual 1410 cm^{-1}).

Sample S01-45 got a clear signal for gypsum in both the portable Raman spectrum as well as in the FTIR-ATR spectrum, so it is quite certain that sample S01-45 primarily consists of gypsum.

The samples for which it was not possible to obtain a clear Raman spectrum (samples P01-23, P08-34, P09-36, S03-40) did yield successful results during FTIR-ATR spectroscopy.

Three out of these four samples displayed a signal for (degraded) cellulose residues, further reinforcing the presence of a significant organic fraction in theses samples. However, due to the nature of FTIR-ATR analysis, it is not clear whether this signal for degraded cellulose stems from the outer layer of the samples (in the form of contamination or biofilm) or if it is a remnant of the original organic fibre that was still preserved inside.

Lastly. Sample P08-34 is the only sample that did not contain either gypsum or calcite like the other samples. Instead, its main mineral component seems to belong to the realm of aluminosilicates (main band at 983 cm^{-1}), possibly representing the presence of plagioclase.

Sample	*Mineral component*	*Organic component*
P01-23	Calcite	Cellulose residues
P02-27	Calcite	Cellulose residues
P03-29	Gypsum	-
P05-31	Gypsum	Organic residue (trace amount)
P07-33	Gypsum	-
P08-34	Aluminosilicates	Organic residue
P09-36	Gypsum	-
S01-45	Gypsum	-
S03-40	Calcite	Cellulose residues
S06-38	Calcite (+ Gypsum? (weak))	-

Table 9: Overview of the FTIR-ATR results. The spectra of all the samples can be found in the appendix (page 76-77).

5.4 X-ray diffraction

XRD proved to be a very useful tool for the identification of the minerals on these samples. Due to aforementioned constraints a selection was made of 6 samples: P01-23, P03-29, P07-33, P09-36, S03-40 and S06-38. When taking a quick glance over the resulting spectra one can already differentiate two groups within the samples. The surface of half of the selected samples consists of mostly, if not almost entirely, of gypsum (figure 20). This is the case for sample P03-29, P07-33, and P09-36, with sample P07-33 also containing some quartz and other sand impurities (3%).

The other group (samples P01-23, S03-40 and S06-38) seems to have one or more forms of calcite as the largest mineral component, though compared to the gypsum group this classifying fraction of calcite is considerably smaller, with the only exception being sample S06-38, which contains a combination of magnesium calcite at 74% and calcite at 26% (figure 21). This presence of both magnesium calcite and calcite likely indicates two generations of calcite formation, where one formed differently perhaps due to the presence of a magnesium source or other materials in the environment (as chemically it is also possible to have manganese or other metals in its matrix). Samples P01-23 and S03-40 do not exhibit signs of two separate calcite formations, as both contain just calcite (P01-23 at 55% and S03-40 at 44%).

*Sample **P01-23***					
Calcite	70%	Quartz (low)	26%	Unknown	4%
*Sample **P03-29***					
Gypsum	100%				
*Sample **P07-33***					
Gypsum	97%	Quartz	3%		
*Sample **P09-36***					
Gypsum	100%				
*Sample **S03-40***					
Calcite	44%	Quartz (low)	36%	Muscovite/ unknown	20%
*Sample **S06-38***					
Magnesium calcite	74%	Calcite	26%		

Table 10: Table containing the XRD results of the selected samples.

Another feature that samples P01-23 and S03-40 share is the considerable present of quartz. Where the one sample from the gypsum group contained only about 3% quartz, over a quarter of the material on samples P01-23 and S03-40 likely consists of quartz (P01-23 at 26% and S03-40). The quartz present in these samples can likely be attributed to sand impurities that made their way into the mineral matrix.

Furthermore, both P01-23 and S03-40 contain a difficult to identify third fraction. For sample P01-23 this is just a small part of about 4%, but for sample S03-40 this comprises a large fraction of about 20%. Most of it could possibly be identified as muscovite, but there is still a peak around 20° 2θ that did not lead to any conclusive identification.

Lastly, most of the spectra display a considerable wide "peak" or in some cases a slope between 0° 2θ and 30° 2θ. This feature is especially present in the samples from the calcite group, but the spectrum for sample P09-36 also displays a distinctive bump with its highest point around 15° 2θ. Such features are caused by amorphous materials which do not cause a diffraction pattern. In this case it could be the result of the presence of organics on these samples, for example degraded cellulose. The wide variety of shapes might be caused by different stages of degradation of cellulose, though a plethora of other factors can influence the pattern as well, such as the possible interaction between the organic and the inorganic components which in turn is affected by the size of the sample, as well as amount of the components present and the ratio between them.

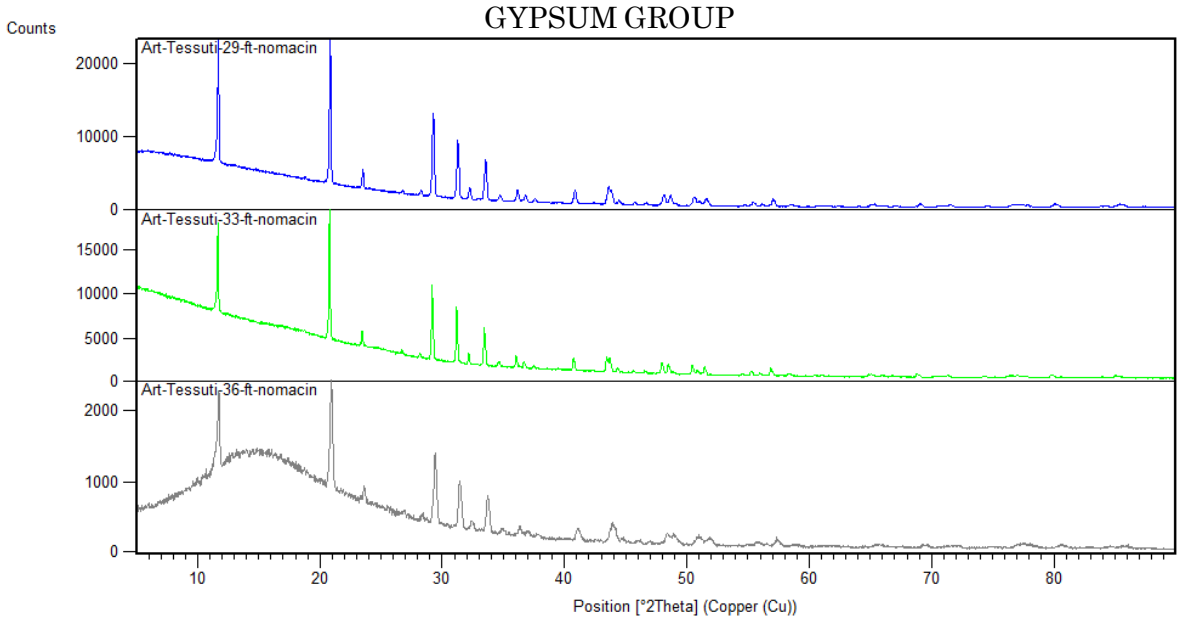

Figure 20: XRD spectra of samples P03-29 (blue), P07-33 (green) and P09-36 (gray). These three samples all contain gypsum, as indicated by the distinctive sharp peaks at 12° 2θ and 21° 2θ, as well as the three consecutive peaks around 29° 2θ, 32° 2θ and 34° 2θ.

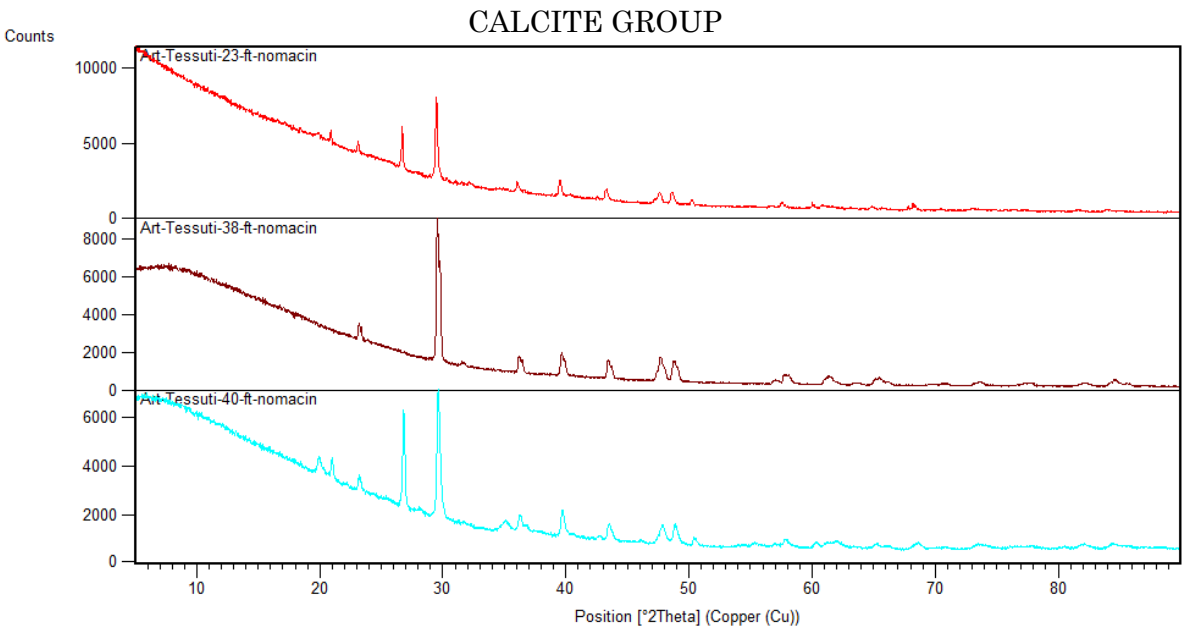

Figure 21: XRD spectra of samples P01-23 (red), S06-38 (brown) and S03-40 (blue). These samples all contain a form of calcite, as indicated by the intense peak around 30° 2θ, as well as the characteristic peaks around 23° 2θ, 36° 2θ, 40° 2θ, 44° 2θ, 48° 2θ and 49° 2θ.

CHAPTER 6:

Discussion

In order to figure out the mineralisation process that preserved these textiles from Perugia, the first step was to identify the mineral fraction. Multiple techniques were employed, not only to get reliable and detailed results, but also to test out different methods for such uncommon material. These different methods covered a couple of bases: Chemical as well as crystallographic information, and analysis of the surface (both in a very small area and all of it in one go) as well as through the entirety of the samples. Almost all of the results obtained using these various methods agree with each other, with some small exceptions (see table 11). Across all methods it became clear that half of the textile samples were covered in (mostly) gypsum, which should not be too surprising as the presence of gypsum has also been reported on the mineralised textile remains from Qatna (Syria) as well as SEM analysis during the previous studies using these samples (James, M. A., Reifarth N., Mukherjee A. J., Crump M. P., Gates P. J., Sandor P., Robertson F., Pfälzner P. & Evershed R. P. 2009; Gleba M. & Vanden Berghe I. 2014). The other half of the samples consist mostly of (magnesium) calcite, although they contain a considerable amount of other minerals as well (unlike the gypsum group, which contains almost exclusively gypsum). Calcite was also to be expected based on results from similar mineralised textiles from Sidon (Lebanon) and previous SEM analysis (Gleba M. & Griffiths D. 2011; Gleba M. & Vanden Berghe I. 2014). There is only one sample that does not fit into either pattern, sample P08-34, which likely contains aluminosilicates instead of gypsum or a form of calcite.

However, not all methods were equally useful when it came to obtaining these results. Especially Raman spectroscopy yielded spotty results. In the beginning there were high hopes for this method, due to its capacity to focus on specific areas and for its theoretical ability to detect organic materials to a degree. For both portable Raman (equipped with a 785 nm laser) and benchtop Raman (equipped with a 514 nm laser) copious amounts of fluorescence occurred, which seemed surprising considering the lack of organic materials observed during the optical analysis of the samples using CLSM, but in hindsight makes more sense as these samples have been exposed to the elements for over 2000 years, likely allowing for patinas to form on the surface.

	Visual group	Mineralisation state	Portable Raman	Benchtop Raman	FTIR-ATR	XRD
P01-23	1	3	n/a	Gypsum	Calcite Cellulose residues	Calcite (70%) Quartz (26%) (4% unknown)
P02-27	1	3	n/a	n/a	Calcite Cellulose residues	n/a
P03-29	3	3	Gypsum	Gypsum	Gypsum	Gypsum (100%)
P05-31	2	3	n/a	n/a	Gypsum Little organic residue	n/a
P07-33	3	2/3	Gypsum	Gypsum (Little calcite?)	Gypsum	Gypsum (97%) Quartz (3%)
P08-34	4	2	n/a	n/a	Aluminosilicates Organic residue	n/a
P09-36	2	3	n/a	n/a	Gypsum	Gypsum (100%)
S01-45	2	3	Gypsum	Gypsum	Gypsum	n/a
S03-40	1	3	n/a	Carbon Black	Calcite Cellulose residues	Calcite (44%) Quartz (36%) (20% unknown – possibly muscovite)
S06-38	4	2	Calcite	n/a	Calcite (shifted)	Magnesium calcite (74%) Calcite (26%)

Table 11: Compilation of all the obtained results across all employed techniques.

These patinas are not the only perceived organics however, as after the poor Raman results the choice was made to perform FTIR-ATR analysis, which picked up signals for organic materials in multiple instances (samples P01-23, P02-27, P05-31, P08-34 and S03-40). Three out of five detected organic residues could be attributed to products of degraded cellulose. Due to the nature of FTIR-ATR, where the IR waves pass through the sample, it is possible that these signals could be remnants of the original fibre of the textiles encased by the minerals, but, at the same time, it is not possible to rule out the possibility that these are the result of organic residues on the surface. In an attempt to determine the cause of this signal we can take a look at the textile technology and see if the signal for cellulose residues corresponds with the possible original fibre following archaeological data (see table 12). Unfortunately, for almost every sample of which the weave type could be identified, no organic residues were detected. The only exception is sample P08-34; however, the organic residues detected on this sample could not be attributed to any organic material in particular, which prevents the identification of the source of these organic residues. Furthermore, as sample S03-40 was located on top of one of the cinerary urns, it is more likely that the cellulose residues might be caused by plant material, which

Sample	*Weave type*	*Possible fibre based on weave type*	*Organic residues (FTIR-ATR)*
P01-23	n/a	-	Cellulose residues
P02-27	n/a	-	Cellulose residues
P03-29	Weft-faced tabby	Wool	n/a
P05-31	n/a	-	Organic residue (trace amount)
P07-33	Balanced tabby	Linen	n/a
P07-33B	Weft-faced tabby	Wool	
P08-34	Weft-faced tabby	Wool	Organic residue
P09-36	n/a	-	n/a
S01-45	n/a	-	n/a
S03-40	n/a	-	Cellulose residues
S06-38	Balanced tabby	Linen	n/a

Table 12: Combination of textile technology data, adapted from Gleba M. & Vanden Berghe I. (2014), and organic residues detected during FTIR-ATR analysis.

could be related to the roots that are visible in the initial image taken from the '*sopra urna*' textile fragments from tomb 29 (figure 8, chapter 3.1.7).

In the end, none of the detected organic residue signals can be convincingly attributed to either the original fibre or outside causes, as with FTIR-ATR analysis the exact location of the detected material is unknown.

As stated before, *almost* all of the results obtained agree with each other, but sample P01-23 is an exception: Benchtop Raman showed a clear signal for gypsum, yet none of the other techniques detected its presence. As mentioned, the FTIR and XRD signal passes through the sample, while Raman only probes the surface. Additionally, Raman spectroscopy, especially the benchtop, only probes a very small area of the sample, while XRD gives a more general impression of the surface makeup. Without the XRD data, one could argue that the formed calcite might have undergone a slow chemical transformation into gypsum due to some possible microbial activity or perhaps other undetermined causes. However, the XRD results did not come up with a signal for gypsum, weakening this hypothesis. Though, on the other hand, as the bench Raman probes a very small area, it could be that it was focused on a particular spot that happened to contain some gypsum, which may not have been detected by XRD due to the relatively miniscule amount of gypsum present or perhaps due to the way the sample was placed inside the instrument.

Another result worth mentioning is that of sample P08-34. Across the used techniques, this sample only yielded one result when it comes to the chemical analysis of the mineral components. It caused too much fluorescence in both of the Raman setups; however, FTIR-ATR did come up with a result, and with a unique one at that: Aluminosilicates (possibly plagioclase), alongside some organic residues. Unfortunately, the FTIR-ATR data for this sample was analysed after the selection for XRD was made, and this sample did not make the cut. In hindsight it would have been very beneficial to have analysed this sample using XRD based on the FTIR-ATR data, as this sample seems to be an exception to the gypsum and calcite seen in the other samples so far, so it would be beneficial for more information to be obtained. It is interesting to note that the broad band around 1000-1020 cm^{-1} seen in most of the FTIR-ATR spectra, which most commonly is a marker for C-O stretching typical for cellulose and cellulose related compounds, can also be related to Si-O stretching in silicates and aluminosilicates, possibly alluding to some type of clay. This could mean that some of the other samples that display this band in their FTIR-ATR spectra do possibly contain aluminosilicates as well, if not for the fact that none of the other analysis techniques picked it up.

Yet another result of the chemical analysis that stands out are the different forms of calcite detected on sample S06-38 during XRD analysis. This might allude to two separate generations of calcite formation, where one might have been formed in contact with other materials, as it is possible for impure calcite to form under such circumstances. Interestingly, the FTIR-ATR spectrum for sample S06-38 in showing the main calcite peaks slightly shifted to a lower wavenumber (main calcite peak of 1410 cm^{-1} now detected at 1395 cm^{-1}), which might be related to this presence of magnesium calcite.
Lastly, in discussing the chemical analysis, is the surprising presence of carbon black on sample S03-40 as detected by benchtop Raman. The aim during Raman spectroscopy was at first to probe every area of interest located with CLSM but was later adjusted to identify the minerals on just the prominent white and dark areas when this initial objective proved to be too challenging. Due to the aforementioned fluorescence problems this new approach was still not successful for all of the samples. Sample S03-40 is the only sample where probing the dark area was successful, with the detection of carbon black as a result. Carbon black, or charcoal black, is a black pigment the use of which is known in Etruscan paintings (Caneva G., Isola D., Lee H. J., & Chung Y. J. 2020). Sample S03-40 was located on top of an urn within tomb 29 of the Strozzacapponi necropolis, which happens to be the richest and most decorated tomb of that necropolis; it is not strange to think that pigments from the polychrome urn made its way into the mineral matrix of the mineralised textile sample found on top of one such urn.

Now that we have an idea of which mineral phases are present on these textiles, it leaves the question as to why they formed there in the first place. The obvious suspect is the abundance of travertine, a carbonate rock, surrounding the samples. Not only the cinerary urns are produced from this rock, but also structural elements of the tombs themselves. This availability of calcium salts from the surrounding travertine, in combination with the limited air circulation, stable temperature and high level of humidity present in subterranean tombs can give rise to physic-chemical weathering, such as efflorescence (Caneva G., Isola D., Lee H. J., & Chung Y. J. 2020). Though it is unclear if there was enough water evaporation inside of the cinerary urns to cause such a strong efflorescence effect on the textiles. Aside from water evaporation, the opposite can also occur: In Etruscan subterranean tombs in Chiusi, the stable microclimate within, in combination with a relative humidity between 90% and 100% resulted in dew point temperature, causing water condensation on surfaces (Caneva G., Isola D., Lee H. J., & Chung Y. J. 2020).

These aforementioned subterranean tomb conditions are ideal for biological weathering in the form of microbial colonisation (CANEVA G., ISOLA D., LEE H. J., & CHUNG Y. J. 2020). Research on biodeterioration within Etruscan tombs indicates that they are mainly populated by various Actinobacteria (order Actinomycetales), as well as Firmicutes (in particular Bacillaceae) and Alphaproteobacteria (order Rhizobiales), which are known to cause white patinas (CANEVA G., ISOLA D., LEE H. J., & CHUNG Y. J. 2020). Such white patinas consist of very fine calcium carbonate crystals (also known as "moonmilk"). (CANEVA G., ISOLA D., LEE H. J., & CHUNG Y. J. 2020). In order to confirm the presence of such biodeterioration in the tombs of Perugia, especially within the cinerary urns, the microbial species present within them should be identified. Furthermore, this type of deterioration mainly explains the presence of calcite, but that leaves the presence of gypsum unaccounted for. Maybe some surface alteration occurred turning calcite into gypsum over time, though there is no strong evidence to support this hypothesis so far. Interestingly, the white calcite patinas reported in Etruscan tombs, did not seem to be that detrimental to the surfaces they occupy, as underneath these patinas wall paintings were relatively well preserved (CANEVA G., ISOLA D., LEE H. J., & CHUNG Y. J. 2020). A similar effect was reported for the painted cinerary urns of Tomba dei Satna in Ponticello, where calcium carbonate crusts preserved the painted decorations.

Another explanation as to why this type of mineralisation occurred stems from Nicole Reifarth, who suggested that the Etruscans may have intentionally added slaked lime (calcium hydroxide) to the burials as part of funerary rituals, which led to carbonatation of the textiles. Furthermore, the basic environment caused by the slaked lime could have facilitated a strong hydrolysis reaction of cellulose, causing the degraded cellulose products detected with FTIR-ATR. Now, as mentioned before, there is no certainty that these cellulosic materials stem from the textiles due to the nature of FTIR-ATR analysis and the lack of data regarding the textile technology of some of the samples, but it could support this theory ever so slightly. Important to note is that other examples of this type of textile mineralisation exist in other areas outside the area occupied by the Etruscans: Both in (Bronze Age) Qatna (Syria) and Sidon (Lebanon), mineralised textile fragments were found in funerary context that were not in contact with metals and contained mainly gypsum and calcite respectively (GLEBA M. & GRIFFITHS D. 2011; JAMES, M. A., REIFARTH N., MUKHERJEE A. J., CRUMP M. P., GATES P. J., SANDOR P., ROBERTSON F., PFÄLZNER P. & EVERSHED R. P. 2009). Moreover, these mineralised textiles, although retrieved from tombs, were not located within cinerary urns like the samples from Perugia. Instead, in Qatna, the mineralised fragments were found on the tomb floor, while at Sidon they were

retrieved from underneath (and near) the backbone of buried remains (GLEBA M. & GRIFFITHS D. 2011; JAMES, M. A., REIFARTH N., MUKHERJEE A. J., CRUMP M. P., GATES P. J., SANDOR P., ROBERTSON F., PFÄLZNER P. & EVERSHED R. P. 2009). Though it is possible that a tradition of adding slaked lime to remains of the deceased could exist across these areas and cultures, it might be more likely that the climatic conditions commonly found in tombs are a more compelling cause for this phenomenon, as all of these specific mineralisation instances share the fact that they were discovered within such contexts. In addition, sample S03-40, that was located on top of one of the urns has also mineralised (into calcite, though this sample contains more 'contamination' in the form of quartz and other materials compared to the other samples). Of course, people could have added the slaked lime solution on top of the urn as well as inside with the cinerary remains, but then we should probably have found more mineralised textiles on top of other urns as well if this were the case.

In an attempt to uncover the mineralisation process multiple techniques have been employed, which in turn lend themselves for a review of the suitability of these techniques for such unusual samples. The CLSM proved to be a useful tool in obtaining clear images of the heavily textured samples. However, the initial plan of localizing areas that display varying degrees of mineralisation using CLSM, to then analyse them using Raman spectroscopy was unsuccessful, due to the advanced stage of mineralisation of the samples (no original organic fibre was present) as well the strong fluorescence in both Raman setups. Still, CLSM might prove useful in archaeological textile research since it has the capability to obtain clear and in-focus images of heavily textured samples at high magnifications, which can aid in identifying various technological parameters of the textiles in question. However, a stereo microscope can also fulfil this task, which is likely a more accessible tool to most researchers. Additionally, SEM could be utilized to obtain sharp images at even greater magnification, a technique which is already commonly employed in textile archaeology to identify the type of fibre. Combining SEM with energy dispersive X-ray (EDS), information on the chemical composition of the sample can be obtained as well, making it a very advantageous technique. In short, CLSM can be very useful in regard to (mineralised) textiles, but it is not a crucial technique within this field as there are better alternatives available.

Then, Raman spectroscopy: Both in a portable setup as well as a benchtop model. This technique turned out to be rather ineffective for most samples, due to a great deal of fluorescence that obstructed the acquisition of clear spectra. At most, only one area of a

sample yielded a readable spectrum, if one could be obtained at all. For the portable Raman, only the white areas came up with a usable spectrum, while the benchtop setup was able to obtain a spectrum for a black area once. Perhaps it would have been better to have used a 785 nm laser with the benchtop Raman as well, as it is more suitable for materials with higher organic contents, mitigating the fluorescence effect to some extent. These fluorescence issues were not foreseen; on paper Raman spectroscopy seemed to be a good choice for identifying the various minerals present on the samples with significant precision thanks to the coupled microscope, as well as its capability to detect organics (to some extent) as well as mineral phases, all while being a non-destructive technique. In hindsight it might seem apparent that archaeological material such as these mineralised textiles contain patinas that have been building up for centuries, as they have been exposed to the elements and various forms of degradation. All in all, Raman spectroscopy proved to be a rather unsuitable technique for this type of material.

In order to counter the poor Raman results, FTIR-ATR analysis was performed. Although micro-destructive, it can detect organic material without the problem of fluorescence. Aside from the main minerals present on the samples, it was able to detect a form of organic residue for five of the samples, though due to the nature of FTIR-ATR, where the infrared waves pass through the samples, it is not possible to ascribe the source of these organic residues with any certainty. It is possible that these residues stem from the textile, but it is just as likely that they are some type of contamination on the outside of the samples. It is rather capable, however, in identifying inorganic phases on these samples, as a spectrum was obtained for all of the samples. But despite this, it might not be a favourable technique for just inorganics identification either, as it is micro-destructive in nature. However, there is a way to employ the FTIR technique in a way that is not destructive: MircoFTIR in External Reflectance (ER-IR) mode does not require contact with the sample. A potential downside to ER-IR technique is that it is less sensitive and possibly biased by spectral distortions.

Lastly, an opportunity arose to perform some final XRD measurements on a selection of the samples. As the samples were inserted whole, the technique was non-destructive, though it must be noted that this method yields slightly less precise results compared to powder diffraction. Nonetheless, some excellent results were obtained for the selected samples, despite the identification of some of the smaller fractions to be quite challenging. It would have been beneficial to analyse all of the samples using XRD, especially in the case of sample P08-34, of which the particular FTIR-ATR result was not known at the time of making the selection. For future investigation of these mineralised textiles, it would be

extremely beneficial to apply XRD to all of the samples, since all the analysed samples yielded useful results, all while being non-destructive. It should be pointed out that only crystals can be properly identified and detected using this technique, which for the identification of the main mineral components did not create any issues, however it would be impossible to determine amorphous or organic materials using XRD.

Though all these techniques combined were adequate to identify the mineral components present on these samples, which was one of the main objectives, the detection of potential organic materials was lacking. Techniques to detect and identify organic material consist of high-performance liquid chromatography (HPLC) and gas chromatography, which are destructive techniques and can therefore not always be employed when working with archaeological or other heritage materials. If the destruction of the mineralised textiles would not be an issue, these two techniques could be employed in order to gather more data on the organic fraction of the samples. Conversely, a different sample preparation could make FTIR more effective. Using chloric acid to destroy the calcium carbonates, for example, will free up the possible organic fraction from the minerals, which can subsequently be analysed using FTIR.

CHAPTER 7:

Conclusion

Using various archaeometric analysis techniques, ten mineralised textile samples taken from Etruscan cinerary urns were investigated in order to uncover the mineralisation process(es) these samples were exposed to, since the usual suspects of textile mineralisation – the presence of metals – were not present within these urns.

These techniques, employed to identify the minerals present on these samples, consisted of Confocal laser scanning microscopy, portable and benchtop Raman spectroscopy, Fourier transform infrared spectroscopy (attenuated total reflectance), and X-ray diffraction, which brought the following observations to light.

The samples can be grouped into three groups based on their main mineral component. The largest group (five samples) contains mainly gypsum ($CaSO_4 \cdot 2H_2O$), followed by four samples containing mainly calcite ($CaCO_3$) (in case of sample S06-38, two forms of calcite could be detected: calcite and magnesium calcite) and lastly one sample, sample P08-34, likely contains Aluminosilicates as its main mineral component, though the data for this sample is not nearly as complete compared to the other samples.

Main mineral	Samples
GYPSUM	P03-29, P05-31, P07-33, P09-36, S01-45
CALCITE	P01-23, P02-27, S03-40, S06-38
ALUMINOSILICATES	P08-34

Table 13: Samples grouped together based on their main mineral component.

These results agree with the SEM-EDS results from a previous study by M. Gleba & I Vanden Berghe (2014) on the mineralised textiles from Strozzacapponi, which also identified both calcite and gypsum. Additionally, textiles mineralised in similar circumstances from Qatna (Syria) and Sidon (Lebanon) seem to contain either gypsum and calcite as well.

Three hypotheses prevail as to how these textiles became mineralised in such a manner; two attribute the cause to natural processes, the other suggests the activity of humans.

Firstly, a case could be made for physic-chemical weathering, in the form of efflorescence that can occur in the high humidity present within Etruscan subterranean tombs. Most of

the material within the tombs – the urns as well as the tombs themselves – are mainly constructed out of Travertine, a carbonate rock. The possible high availability of calcium salts of the Travertine in combination with the microclimate within the tombs might have resulted in efflorescence in the form of carbonatation.

Secondly, another type of weathering process could have possibly caused this type of mineralisation, brought forth by another culprit: bacteria and other microbes. Research conducted at other Etruscan necropoleis (Chiusi and Tarquinia), which identified different microbial species that made the tombs their home, found that species of Actinobacteria, Firmicutes and Alphaproteobacteria formed a significant part of the occupants. These species cause a form of biological weathering that results in white patinas mainly consisting of very fine calcium carbonate crystals. Though no microbes have been identified in the tombs of Perugia in previous research nor in this thesis, it might be an interesting next step in further research into this topic.

Lastly, human activities in the form of addition of slaked lime to the remains of the deceased, as first suggested by Nicole Reifarth in 2022, forms another possible hypothesis. This addition of slaked lime (calcium hydroxide) in turn can cause a carbonatation reaction, resulting in the formation of calcite. Furthermore, slaked lime provides a very basic environment capable facilitating a strong hydrolysis reaction of cellulose, which might be the cause of the detected cellulose residues during FTIR-ATR analysis (samples P01-23, P02-27 and S03-40), though due to the nature of FTIR-ATR it cannot be confirmed that these residues actually stem from the textile as it is also possible that the cellulose and other organic residues are contaminants on the surface on the samples. However, if Etruscans added slaked lime as part of their funerary practice, then this raises the question if this practise also existed in Bronze Age Syria and Lebanon, as similarly mineralised textiles were found there. It might therefore be more likely that the tomb environments these mineralised textiles were preserved in is one of the main factors of this type of mineralisation, as this is a recurring factor among all three instances.

There is a problem, however, with all three hypotheses. They all provide an explanation for the presence of calcite, yet half of the samples contain primarily gypsum. It remains unclear why this is the case, perhaps the calcite underwent some type of alteration resulting in the transformation into gypsum, though this must be explored more in future research.

For the analysis of the mineralised textile samples multiple techniques were employed, with varying rates of success. CLSM proved to be a useful tool for mapping the surface of

the samples but did not turn out to be a crucial to the overall analysis. Raman spectroscopy was expected to be a very useful tool, but due to unforeseen difficulties caused by strong fluorescence, it was rather ineffective and for this reason would not be recommended for further research into this topic. On the other hand, FTIR-ATR and XRD were indispensable for the analysis. Both techniques resulted in useful data regarding the mineral contents of the samples, but it must be stated that FTIR-ATR is a micro-destructive technique and it is therefore not always applicable, though this could be bypassed by using MircoFTIR in External Reflectance (ER-IR) mode instead. Furthermore, the IR waves of FTIR-ATR pass though the samples, probing the surface as well as the interior of the sample, which proved to be rather troublesome since the organic residues detected for some the mineralised textiles could not be pinpointed. XRD functioned very well, though it is not perfect as it cannot be used to identify organic and amorphous materials. Still, it would be beneficial to apply XRD analysis to all of the samples instead of just a selection. All in all, multiple techniques should be combined in order to obtain a more complete image of mineralised textiles and their chemical makeup. Techniques already in use in the field of textile archaeology, especially SEM-EDS, should be included into this type of research, as it has been proved useful in previous studies. Furthermore, techniques such as high-performance liquid chromatography (HPLC) and gas chromatography could be employed to better analyse the organic fraction of such samples. Conversely, a different sample preparation could make FTIR more effective in regard to detecting organic materials. These methods are destructive in nature and therefore not always applicable to cultural heritage materials.

To conclude, the exact causes of this type of mineralisation remain unclear, both natural as well as human factors could have played a role in the transformation of textiles into gypsum and calcite. To better understand this process, future studies could address the climatic conditions present within the tombs of Ponticello and Strozzacapponi, as well as investigate any microbial presence in the vicinity of the mineralised textiles. Lastly, more archaeological and chemical evidence is needed to successfully determine if human activity, for instance the addition of slaked lime, is responsible for the preservation of these textiles in a mineralised state.

Bibliography

ADOVASIO J. M., SOFFER O. & KLÍMA B. 1996. *Upper palaeolithic fibre technology: Interlaced woven finds from Pavlov I, Czech Republic, c. 26,000 years ago*. Antiquity, 70(269), 526.

BARTOLONI G. 2012. *Introduzione all'etruscologia*. Milano.

BENDER JØRGENSEN L. 2004. *A matter of material: changes in textiles from Roman sites in Egypt's Eastern Desert*. Antiquité tardive, 12, 87-99.

BIZZARRI R., MELELLI L. & CENCETTI C. 2018. *Archaeo-geosites in urban areas: A case study of the Etruscan Palazzone Necropolis (Perugia, central Italy)*. Alp. Mediterr. Quat, 31, 1-12.

CANEVA G., ISOLA D., LEE H. J. & CHUNG, Y. J. 2020. *Biological risk for hypogea: Shared data from Etruscan tombs in Italy and ancient tombs of the Baekje dynasty in Republic of Korea*. Applied Sciences, 10(17), 6104.

CECCARELLI L. 2016. *The Romanization of Etruria*, in Bell, S., & Carpino, A. A. (Eds.), *A Companion to the Etruscans*, John Wiley & Sons, pp. 28-40

CECCARELLI L. & STODDART S. 2021. *Perugia: the frontier city*, in GLEBA M., BEATRIZ M. A., & BELA D (eds.), *Making Cities: Economies of Production and Urbanisation in Mediterranean Europe 1000-500 BC*. McDonald Institute Monographs, pp. 161-175.

CENCIAIOLI L., & FERUGLIO A. E. 2004. *Il piacere della seduzione: materiali dalle necropoli perugine*. Soprintendenza per i beni archeologici dell'Umbria.

CHEN H. L., JAKES K. A., & FOREMAN D. W. 1998. *Preservation of archaeological textiles through fibre mineralization*. Journal of Archaeological Science, 25(10), 1015-1021.

CONKLIN W. J. & CONKLIN B. M. 2007. *An Aguada textile in an Atacamenian context*. Andean Past, 8(1), 21.

CYBULSKA M. & MAIK J. 2007. *Archaeological textiles–a need for new methods of analysis and reconstruction.* Fibres and Textiles in Eastern Europe, 15(5-6), 185-189.

DOWSETT M., WIESINGER R. & ADRIAENS M. 2021. *X-Ray diffraction*. Spectroscopy, diffraction and tomography in art and heritage science, Elsevier 45-69.

GLEBA M. 2016. *Etruscan textiles in context*, in BELL S., & CARPINO A. A. (Eds.), *A Companion to the Etruscans*, John Wiley & Sons, 237-246.

GLEBA M. 2017a. *Textiles in pre-Roman Italy: from a qualitative to a quantitative approach*. Origini XL, (40), 9-28

GLEBA M. 2017b. *Tracing textile cultures of Italy and Greece in the early first millennium BC*. Antiquity, 91(359), 1205-1222

GLEBA M., & GRIFFITHS D. 2011. *Textile remains from a Middle Bronze Age burial in Sidon*. Archaeology & history in Lebanon, (34-35), 285-296.

GLEBA M., & Mannering U. 2012. *Textiles and textile production in Europe from prehistory to AD 400*. Oxbow Books.

GLEBA M. & VANDEN BERGHE I. 2014. *Textiles from Strozzacapponi (Perugia/Corciano). New evidence of purple production in pre-Roman Italy.* Production and Trade of Textiles and Dyes in the Roman Empire and Neighbouring Regions. València, 167-17.

GLEBA M., VANDEN BERGHE I. & CENCIAIOLI L. 2017. *Purple for the masses? Shellfish purple-dyed textiles from the quarry workers' cemetery at Strozzacapponi (Perugia/Corciano), Italy,* in ENEGREN H. L., & MEO F. (Eds.), *Treasures from the Sea. Oxbow Books Treasures from the sea: sea silk and shellfish purple dye in antiquity*, Oxbow Books, 131-137.

GRIFFITHS P.R. & DE HASETH J. A. 2007. *Fourier transform infrared spectrometry* (Second edition). Wiley-Interscience.

GOOD I. 2001. *Archaeological textiles: a review of current research*. Annual Review of Anthropology, 30(1), 209-226.

HAN J. I. 2011. *A study on the characteristics of the designs on Coptic textiles of Ancient Egypt*. Journal of Fashion Business, 15(3), 112-124.

HAYNES S. 2000. *Etruscan civilization: a cultural history*. Getty Publications.

HOSKINS N. A. 2011. *Woven Patterns on Tutankhamun Textiles*. Journal of the American Research Center in Egypt, 199-215.

IZZET V. 2007. *The archaeology of Etruscan society*. Cambridge University Press.

JAKES K. A. & SIBLEY L. R. 1984*. An examination of the phenomenon of textile fabric pseudomorphism*. Archaeological Chemistry III, 403-424.

JAMES M. A., REIFARTH N., MUKHERJEE A. J., CRUMP M. P., GATES P. J., SANDOR P., ROBERTSON F., PFÄLZNER P. & EVERSHED R. P. 2009. *High prestige Royal Purple dyed textiles from the Bronze Age royal tomb at Qatna, Syria*. Antiquity, 83(322), 1109-1118.

KING M. E. 1978. *Analytical methods and prehistoric textiles*. American Antiquity, 43(1), 89-96.

LEIGHTON R. 2005. *House urns and Etruscan tomb painting: tradition versus innovation in the ninth–seventh centuries BC*. Oxford journal of archaeology, 24(4), 363-380.

LIU G. L., & KAZARIAN S. G. 2022. *Recent advances and applications to cultural heritage using ATR-FTIR spectroscopy and ATR-FTIR spectroscopic imaging*. Analyst, 147(9), 1777-1797.

MANNERING U., POSSNERT G., HEINEMEIER J., & GLEBA M. 2010. *Dating Danish textiles and skins from bog finds by means of 14C AMS.* Journal of Archaeological Science, 37(2), 261-268.

MARÍN-AGUILERA B., IACONO F. & GLEBA M. 2018. *Colouring the Mediterranean: Production and consumption of purple-dyed textiles in pre-roman times*. Journal of Mediterranean Archaeology, 31(2), 127-154.

NEIL S. 2016. *Materializing the Etruscans: The Expression and Negotiation of Identity during the Orientalizing, Archaic, and Classical Periods*, in BELL S., & CARPINO A. A. (Eds.), *A Companion to the Etruscans*, John Wiley & Sons, 15-27.

NWANESHIUDU A., KUSCHAL C., SAKAMOTO F. H., ANDERSON R. R., SCHWARZENBERGER K. & YOUNG R. C. 2012. *Introduction to confocal microscopy*. Journal of Investigative Dermatology, 132(12), 1-5.

PASTONCHI L., PALLECCHI P., FORESI L. M., BAMBINI A. M. & ROSSATO L. 2015. *Produzioni etrusche in pietra fetida nell'Etruria settentrionale: materie prime e loro provenienza*. Notiziario della Soprintendenza per i Beni Archeologici della Toscana: 11, saggi, 2015, 59-66.

ROUSAKI A. & VANDENABEELE P. 2021. *Raman and infrared spectroscopy in conservation and restoration*, in ADRIAENS M. & DOWSETT M. (Eds.), *Spectroscopy, diffraction and tomography in art and heritage science*. Elsevier, 45-69.

RUBINSON K. S. 1990. *The textiles from Pazyryk*. Expedition, 32(1), 49.

SCHMIDT-COLINET A. 1995. *The Textiles from Palmyra*. ARAM Periodical, 7(1), 47-51.

SCIAU P. & GODET M. 2021. *Spectroscopy and diffraction using the electron microscope*, in ADRIAENS M. & DOWSETT M. (Eds.), *Spectroscopy, diffraction and tomography in art and heritage science*. Elsevier, 71-102.

SEMWOGERERE D. & WEEKS E. R. 2005. *Confocal microscopy*. Encyclopedia of biomaterials and biomedical engineering, 23, 1-10.

SMITH C. 2014. *The Etruscans: a very short introduction*. Oxford University Press, USA.

Smith, G. D., & Clark, R. J. (2004). Raman microscopy in archaeological science. *Journal of archaeological science*, 31(8), 1137-1160.

STEINGRÄBER S. 2020. *Etruscan Tombs*, in SMITH C. (eds). *Encyclopedia of Global Archaeology*. Springer, Cham., 10646–10657.

STEINGRÄBER S. 2016. *Rock Tombs and the World of the Etruscan Necropoleis: Recent Discoveries, Research, and Interpretations*, in BELL S., & CARPINO A. A. (Eds.), *A Companion to the Etruscans*, John Wiley & Sons, 146-161.

STODDART S. 2016a. *Beginnings: Protovillanovan and Villanovan Etruria*, in BELL S., & CARPINO A. A. (Eds.), *A Companion to the Etruscans*, John Wiley & Sons, 1-14.

STODDART S. (2016b). *City and Countryside*, in BELL S., & CARPINO A. A. (Eds.), *A Companion to the Etruscans*, John Wiley & Sons, 55-66.

TENG X., LI F. & LU C. 2020. *Visualization of materials using the confocal laser scanning microscopy technique*. Chemical Society Reviews, 49(8), 2408-2425.

WIMAN I. M. 2014. *Etruscan environments*, in TURFA J. M. (Eds.), *The Etruscan World. Routledge*, 59-76.

ZHANG X., GOOD I., & LAURSEN R. 2008. *Characterization of dyestuffs in ancient textiles from Xinjiang*. Journal of Archaeological Science, 35(4), 1095-1103.

Appendix

No.	Old sample no.	Combined no.	Site	Context		Material	Colour
P01	23	P01-23	Ponticello (Perugia)	Tomba dei Satna	Urn 2	Textile	Dark grey
P02	27	P02-27	Ponticello (Perugia)	Tomba dei Satna	Urn 2	Textile	Light brown / beige
P03	29	P03-29	Ponticello (Perugia)	Tomba dei Satna	Urn 3	Textile	White
P04	30	P04-30	Ponticello (Perugia)	Tomba dei Satna	Urn 3	Soil	Brown
P05	31	P05-31	Ponticello (Perugia)	Tomba dei Satna	Urn 4	Textile	Beige
P06	32	P06-32	Ponticello (Perugia)	Tomba dei Satna	Urn 4	Soil	Light brown / beige
P07	33	P07-33	Ponticello (Perugia)	Tomba dei Satna	Urn 6	Textile	White
P07-B	33	P07-33B	Ponticello (Perugia)	Tomba dei Satna	Urn 6	Textile	White
P08	34	P08-34	Ponticello (Perugia)	Tomba dei Satna	Urn 6	Textile	Brown
P08-B	34	P08-34B	Ponticello (Perugia)	Tomba dei Satna	Urn 6	Textile	Brown
P09	36	P09-36	Ponticello (Perugia)	Tomba dei Satna	Urn 7	Textile	White
P10	37	P10-37	Ponticello (Perugia)	Tomba dei Satna	Urn 7	Soil	Brown & white
S01	45	S01-45	Strozzacapponi (Corciano, Perugia)	Tomb 27	Urn 215166	Textile	White
S01-B	45	S01-45B	Strozzacapponi (Corciano, Perugia)	Tomb 27	Urn 215166	Textile	White
S02	26	S02-26	Strozzacapponi (Corciano, Perugia)	Tomb 27	Urn 215166	Textile	Dark grey
S03	40	S03-40	Strozzacapponi (Corciano, Perugia)	Tomb 29	Sopra Urna	Textile	Grey-ish brown
S04	25	S04-25	Strozzacapponi (Corciano, Perugia)	Tomb 29	Sopra Urna	Textile	Drak grey
S05	42	S05-42	Strozzacapponi (Corciano, Perugia)	Tomb 29	Sopra Urna	Soil	-
S06	38	S06-38	Strozzacapponi (Corciano, Perugia)	Tomb 29	Urn 5	Textile	Purple & white, dark grey*

Table 14: Complete sample list

No.	Old sample no.	Combined no.	No. of fragments	Approx. Length	Approx. Width	Notes
P01	23	P01-23	5	< 4 mm	< 4 mm	One small fragmet + 5 small pieces on sample holder (<5 mm)
P02	27	P02-27	1	10 mm	5 mm	
P03	29	P03-29	> 5*	10 mm	4 mm	*Multiple smaller pieces present in bag
P04	30	P04-30	-	-	-	
P05	31	P05-31	1	10 mm	6 mm	
P06	32	P06-32	-	-	-	
P07	33	P07-33	1	9 mm	4 mm	Two fragments in same tube (P07-33B) + 1 fragment on sample holder (<4 mm)
P07-B	33	P07-33B	1	6 mm	5 mm	
P08	34	P08-34	1	10 mm	7 mm	Two fragments in one bag (P08-34B), FRAGILE (crumbly)
P08-B	34	P08-34B	1	10 mm	5 mm	
P09	36	P09-36	1	20 mm	16 mm	
P10	37	P10-37	-	-	-	
S01	45	S01-45	1	20 mm	15 mm	Two fragments in one bag (S01-45B)
S01-B	45	S01-45B	1	16 mm	10 mm	
S02	26	S02-26	3	6 mm	6 mm	Sample taken from S01-45, on sample holder
S03	40	S03-40	1	10 mm	7 mm	
S04	25	S04-25	2*	< 4 mm	< 4 mm	Sample taken from S03-40, *2 small pieces on sample holder (<4 mm)
S05	42	S05-42	-	-	-	
S06	38	S06-38	2	10 mm, 10 mm*	5 mm, 1 mm*	First fragment folded, *second fragment on sample holder

Continuation of table 14

FTIR-ATR SPECTRA

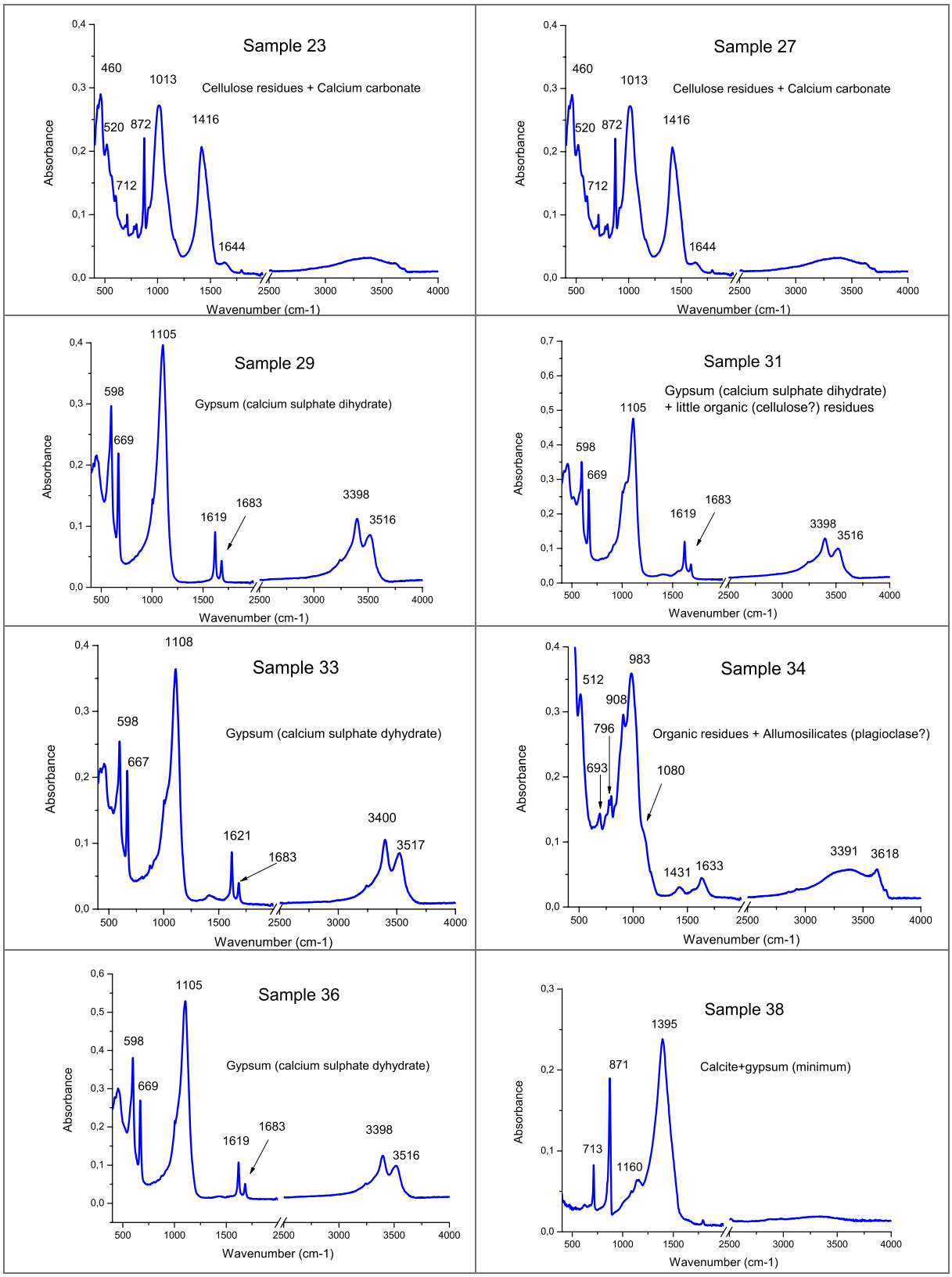

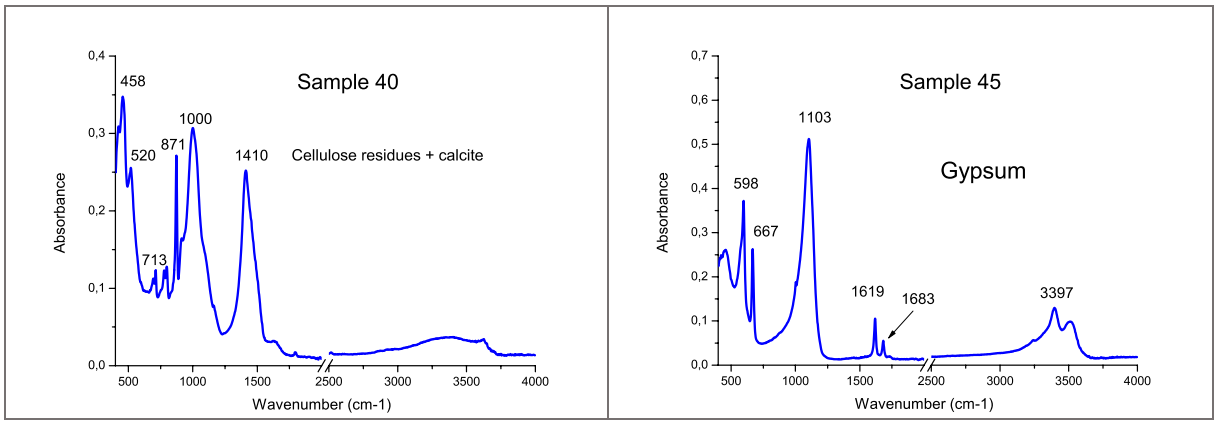

FTIR-ATR Spectra have been made by prof. A. Zoleo of the Department of Chemical Sciences of the University of Padua